

1 **Methane, ethane, and propane production in Greenland ice**
2 **core samples and a first isotopic characterization of excess**
3 **methane**

4 Michaela, Mühl¹, Jochen Schmitt¹, Barbara Seth¹, James E. Lee², Jon S. Edwards³, Edward J.
5 Brook³, Thomas Blunier⁴, Hubertus Fischer¹

6
7 ¹Climate and Environmental Physics and Oeschger Centre for Climate Change Research, University of Bern,
8 Bern, 3012, Switzerland

9 ²Los Alamos National Laboratory, Earth Systems Observation, Los Alamos, NM 87545, USA

10 ³College of Earth, Ocean, and Atmospheric Sciences, Oregon State University, Corvallis, OR 97331, USA

11 ⁴Centre for Ice and Climate, Niels Bohr Institute, University of Copenhagen, Copenhagen, 2200, Denmark

12

13 *Correspondence to:* Michaela Mühl (michaela.muehl@unibe.ch)

14

15

16

17

18

19

20

21

22

23

24

25

26

27

28

29

30

31

32

33

34

35

36 **Abstract.** Air trapped in polar ice provides unique records of the past atmospheric composition
37 ranging from key greenhouse gases such as methane (CH₄) to short-lived trace gases like ethane
38 (C₂H₆) and propane (C₃H₈). Recently, the comparison of CH₄ records obtained using different
39 extraction methods revealed disagreements in the CH₄ concentration for the last glacial in
40 Greenland ice. Elevated methane levels were detected in dust-rich ice core sections measured
41 discretely pointing to a process sensitive to the melt extraction technique. To shed light on the
42 underlying mechanism, we performed targeted experiments and analyzed samples for methane
43 and the short-chain alkanes ethane and propane covering the time interval from 12 to 42 kyears.
44 Here, we report our findings of these elevated alkane concentrations, which scale linearly with
45 the amount of mineral dust within the ice samples. The alkane production happens during the
46 melt extraction step of the classic wet extraction technique and reaches 14 to 91 ppb of CH₄
47 excess in dusty ice samples. We document for the first time a co-production of excess methane,
48 ethane, and propane with the observed concentrations for ethane and propane exceeding their
49 past atmospheric background at least by a factor of 10. Independent of the produced amounts,
50 excess alkanes were produced in a fixed molar ratio of approximately 14:2:1, indicating a
51 shared origin. The carbon isotopic signature of excess methane is $(-47.0 \pm 2.9) \text{‰}$ and its
52 deuterium isotopic signature is $(-326 \pm 57) \text{‰}$ in the samples analyzed. With the co-production
53 ratios of excess alkanes and the isotopic composition of excess methane we established a
54 fingerprint that allows us to constrain potential formation processes. This fingerprint is not in
55 line with a microbial origin. Moreover, an adsorption-desorption process of thermogenic gas
56 on dust particles transported to Greenland appears not very likely. Rather the alkane pattern
57 appears to be indicative of abiotic decomposition of organic matter as found in soils and plant
58 leaves.

59 **1. Introduction**

60
61 Atmospheric air entrapped in polar ice represents a unique archive of the past atmospheric
62 composition including the concentration of greenhouse gases like carbon dioxide (CO₂)
63 methane (CH₄) and nitrous oxide (N₂O) but also short-lived trace gases such as ethane (C₂H₆)
64 and propane (C₃H₈). The ongoing anthropogenic increase in the atmospheric concentrations of
65 these gases makes a detailed understanding of their preindustrial variations and biogeochemical
66 cycling of paramount importance and only polar ice cores are able to provide this information.
67 However, to interpret reconstructions of the atmospheric composition from polar ice cores
68 requires that archived atmospheric trace gases are not altered within the ice itself. Furthermore,
69 the air must be extracted from the ice sample without altering the original composition. Thus,

70 the comparison of ice core records obtained using different extraction techniques and from
71 different ice cores requires careful consideration and interpretation.

72
73 It is known that not all drill sites or specific time intervals are equally suitable to derive pristine
74 atmospheric trace gas records. For example CO₂ data from Greenland ice are subject to CO₂ in
75 situ production due to impurities in the ice (Anklin et al., 1995; Smith et al., 1997). In situ
76 production is also observed for N₂O, for example in glacial Antarctic ice core samples
77 characterized by higher dust content (Schilt et al., 2010). In contrast, CH₄ in polar ice cores, in
78 the absence of melt layers, was considered to be not affected by such in situ processes.
79 However, more recent results from Greenland showing elevated CH₄ concentrations in glacial
80 dust-rich ice (Lee et al., 2020) and high amplitude CH₄ spikes in Holocene ice (Rhodes et al.,
81 2013, 2016) question this assumption.

82
83 This becomes especially worrisome as atmospheric methane shows a significant North-South
84 gradient, reflecting the predominance of Northern Hemisphere sources. Ice cores from
85 Greenland and Antarctica have been used to quantify this Inter-Polar Difference (IPD) in past
86 CH₄ concentrations (Chappellaz et al., 1997; Baumgartner et al., 2012, Beck et al., 2018) with
87 the goal to derive the relative contribution of Northern and Southern hemispheric sources to the
88 overall CH₄ changes. The Holocene IPD is on the order of several tens of ppb, i.e., one order
89 of magnitude smaller than the past atmospheric CH₄ concentration. Thus, any small CH₄ bias
90 on the order of a few ppb to tens of ppb has a strong impact on the conclusions drawn from this
91 IPD, while the influence on the total radiative forcing by such small biases is negligible. In
92 summary, existing results of CH₄ concentrations from Greenland and Antarctic ice cores have
93 to be carefully scrutinized for such effects.

94
95 A first step in this direction has been made in previous work by Lee et al. (2020), for example
96 by comparing CH₄ records derived using different measurement techniques. Past CH₄
97 concentrations ([CH₄]) are retrieved by measurements of Greenland and Antarctic ice cores
98 using traditional discrete and relatively new continuous melt extraction techniques. While
99 discrete ice measurements deliver one single value for each sample, Continuous Flow Analyses
100 (CFA) gradually melt a thin stick of the ice core providing a continuous record for this section.
101 Although in both techniques the ice sample is melted, the CFA technique separates air from the
102 meltwater stream in about 1-2 min providing only a short time for any reaction in the water
103 while for the discrete technique the contact time is typically 15-30 min. Comparing [CH₄]

104 histories from several Greenland ice cores measured discretely (NGRIP, GISP2, GRIP) with
105 the continuous Greenland NEEM and the continuous Antarctic WAIS records over the last
106 glacial period, higher [CH₄] can be found in the discrete Greenland measurements for specific
107 time intervals (Lee et al., 2020; Fig. 1 therein), where dust concentrations are especially high.

108

109 Looking at the NGRIP methane hydrogen isotope ($\delta\text{D-CH}_4$) record (Bock et al., 2010b), which
110 was also measured with a discrete melt extraction technique (Bock et al., 2010a), it turns out
111 that in the high dust ice sections, the isotopic values are also affected. Several negative
112 hydrogen isotopic excursions with a maximum depletion of 16 ‰ (permil) prior to the onset of
113 Dansgaard-Oeschger (DO) event 8 were identified (Bock et al., 2010b). At the time of that
114 publication there was no straightforward explanation for these depletions that could lead to
115 “lighter” $\delta\text{D-CH}_4$ values during times of a relatively stable climate. Using ice from Antarctica
116 much smaller $\delta\text{D-CH}_4$ variations (3-4 ‰) during this interval were found in measurements
117 performed at the University of Bern (unpublished data), again questioning the atmospheric
118 origin of these $\delta\text{D-CH}_4$ depletions prior to the DO onset.

119

120 All these variations recorded in Greenland ice give reason to assume that a hitherto unknown
121 process exists that produces or releases additional methane in some time intervals in Greenland
122 ice cores (from here on referred to as “excess methane” or CH_{4(xS)}). This process is related to
123 the extraction technique (only found in records obtained by discrete melt extractions) and has
124 only been observed in glacial Greenland ice with high mineral dust concentrations.

125

126 A first attempt to characterize CH_{4(xS)} was made by Lee et al. (2020) who analyzed [CH₄] in
127 discrete ice samples with different impurity composition and concentration from several ice
128 cores (GISP2, NEEM, WAIS, SPICE) using a multiple melt-refreeze technique. They were able
129 to quantify CH_{4(xS)} contributions of up to 30-40 ppb for Greenland samples. Sequential melt-
130 refreeze extractions showed that the process leading to CH_{4(xS)} is slow and not completed during
131 the first melt-refreeze cycle (i.e., within around 30 min). A special set of samples was analyzed
132 with the admixture of a HgCl₂ solution to suppress microbial activity in the meltwater. No
133 difference in the measured [CH₄] was observed between the poisoned samples and replicates
134 without HgCl₂, excluding a microbial CH₄ production after melting. In addition, Lee et al.
135 (2020) used the NGRIP [CH₄] (Baumgartner et al., 2014) and $\delta\text{D-CH}_4$ records (Bock et al.,
136 2010b) to estimate the deuterium isotopic signature of the CH_{4(xS)}. Assuming a two-component

137 mixture of atmospheric methane and excess methane their model led to a best estimate of (-293
138 ± 31) ‰ for δD -CH_{4(xs)}.

139

140 A straightforward explanation for CH_{4(xs)} may be that CH₄ is either produced in the meltwater,
141 or it was produced beforehand and only released during the melt extraction. With respect to
142 that, Lee et al. (2020) reviewed several mechanisms that could account for the observed
143 variations in Greenland ice core records. None perfectly matched all their observations but
144 lastly, three of the proposed mechanisms were short-listed by Lee et al. (2020): (1) an
145 adsorption process on dust particles prior to the deposition on the ice sheet; (2) an in situ
146 production in the ice; or (3) an abiotic reaction during melt extraction.

147

148 Here we resume the work by Lee et al. (2020) and shed more light upon the potential formation
149 processes using a targeted and more comprehensive study to quantify CH_{4(xs)}. We analyzed
150 specific NGRIP and GRIP ice core samples discretely with two different wet extraction
151 systems. With our $\delta^{13}C$ -CH₄ device we are able to measure [methane], [ethane], [propane], and
152 $\delta^{13}C$ -CH₄ on a single ice sample in two subsequent extractions. With our second device we add
153 experimental information on δD -CH₄. In Sect. 2 we provide information on our sampling
154 strategy and measurement techniques. With our new experimental results, presented in Sect. 3,
155 we provide quantitative data for CH_{4(xs)} in NGRIP and GRIP samples and extend our
156 observations to other “excess alkanes” (ethane and propane), which are revealed to be co-
157 produced during the excess CH₄ production. The observed molar ratios between methane,
158 ethane, and propane are evaluated and their relation to the abundance of mineral dust (Ca²⁺)
159 within the ice samples is quantified. A 2nd extraction of the meltwater enables us to estimate
160 the temporal dynamics of excess alkane production. Using a Keeling-plot approach to our
161 isotopic results, we calculate the carbon and deuterium isotopic signature of excess CH₄ ($\delta^{13}C$ -
162 CH_{4(xs)} and δD -CH_{4(xs)}). Based on our new and improved evidence, we finally come back to the
163 discussion of the hypotheses proposed by Lee et al. (2020) in Sect. 4 and offer potential
164 mechanisms that could explain the excess alkanes in ice core samples. For readers not interested
165 in all the experimental details, we recommend to jump straight to Sect. 4 to see the disussion.

166

167 **2. Ice core samples and measurements**

168 **2.1 Ice core samples**

169

170 Mixing ratios of alkanes (methane, ethane, and propane) and the stable carbon ($\delta^{13}\text{C}-\text{CH}_4$) and
171 hydrogen ($\delta\text{D}-\text{CH}_4$) isotope ratios of methane were measured on ice core samples from the
172 North Greenland Ice Core Project (NGRIP) ice core. For this study, a total of 19 NGRIP ice
173 core samples were measured for $\delta^{13}\text{C}-\text{CH}_4$ and alkane concentrations and nine NGRIP ice
174 samples for $\delta\text{D}-\text{CH}_4$ covering the depth between 1795.84 m and 1933.25 m. The NGRIP
175 samples are from the late glacial Marine Isotope Stages (MIS) 3 and 2 (22.6 to 30.6 kyears BP).
176 These time intervals are characterized by sharp atmospheric CH_4 increases in parallel to rapid
177 warmings, the so-called Dansgaard-Oeschger events, but we mostly sampled intervals with
178 stable CH_4 concentrations. From the same time period, we also investigate measurements of 41
179 NGRIP and 12 GRIP ice core samples which were carried out in 2011 and 2018, respectively,
180 and which have not previously been published. See Fig. 1 for an overview of all analyzed
181 NGRIP and GRIP ice core samples over time.

182

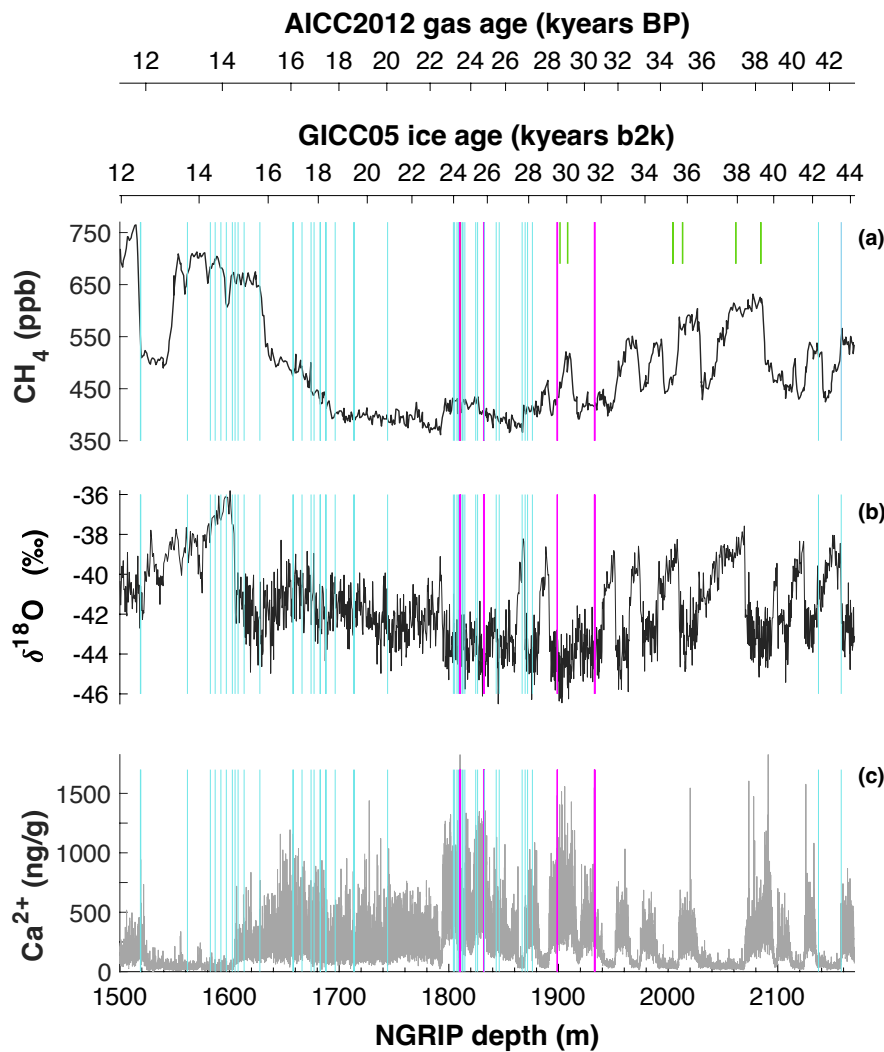
183 We also included 22 ice core samples from the European Project for Ice Coring in Antarctica
184 (EPICA) ice core from Dome C (MIS 4), which are not affected by a measureable excess CH_4
185 production and which we use as long-term monitoring ice for the system performance and to
186 quantify the blank contribution of the analytical system (see Appendix B).

187 The late glacial time period, which includes the age of most of the measured NGRIP samples,
188 is characterized by an overall high impurity and dust content and low atmospheric methane
189 concentrations. For our analysis, we have selected ice core bags (where for NGRIP and GRIP
190 ice cores, a bag is a 55 cm long ice core section) in which we expect the same atmospheric CH_4
191 concentration but see a high range of mineral dust content (Ca^{2+}). In this way we can compare
192 neighbouring samples that have the same low stadial CH_4 levels due to stable atmospheric
193 concentrations and temporal smoothing by the slow bubble enclosure process but are expected
194 to vary in measured concentrations due to contributions of excess alkanes. Ca^{2+} content across
195 our NGRIP samples range from 307 ng/g to 1311 ng/g. This sample selection is also critical to
196 quantify the isotopic signature of the $\text{CH}_{4(\text{xs})}$ produced using the Keeling-plot approach
197 (Keeling, 1958). The underlying assumptions of this mass balance approach are that (1) there
198 is only a two-component mixture (atmospheric methane and excess methane) and that (2) the
199 isotopic ratio of the mixture changes only by a varying input of the second source ($\text{CH}_{4(\text{xs})}$).

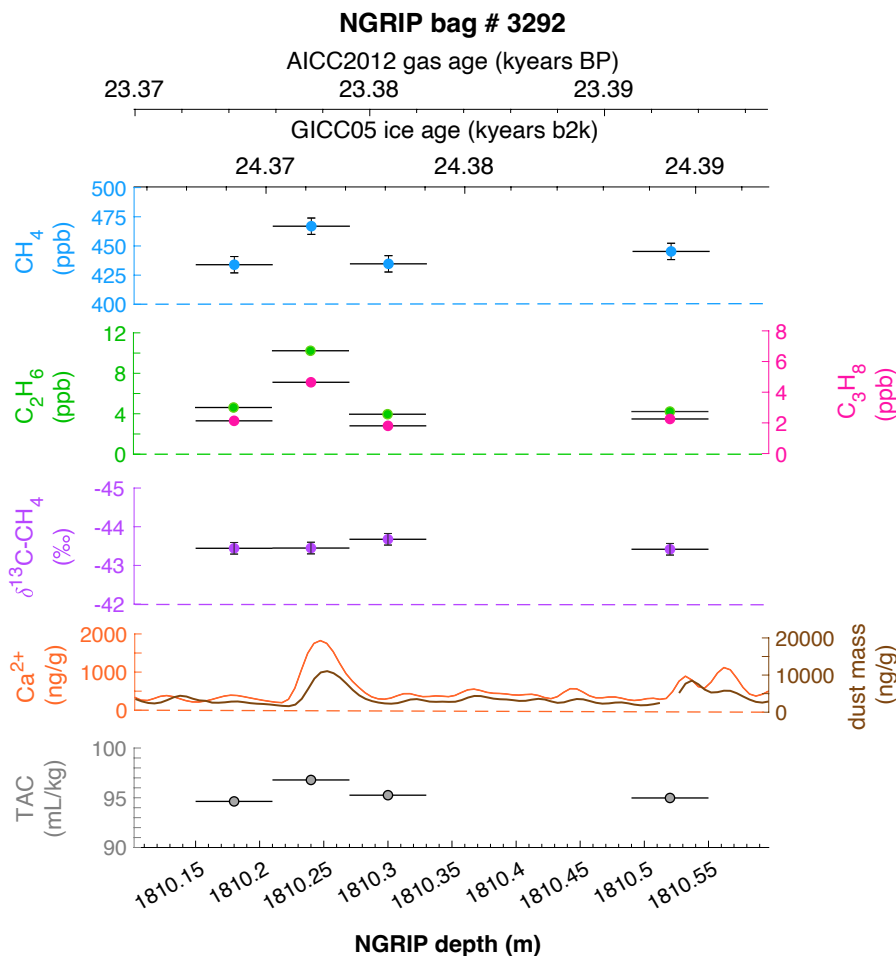
200

201 To select the samples, we use high-resolution mineral dust records measured using an Abakus
202 laser attenuation device (Klotz, Germany) for particulate dust (Ruth et al., 2003) as well as Ca^{2+}
203 concentrations (Erhardt et al., 2022) as dissolved mineral dust tracer derived from the Bern

204 Continuous Flow Analysis System (Kaufmann et al., 2008) . In principle, particulate dust and
 205 the specific soluble dust tracer Ca^{2+} are strongly correlated. However, depending on acidity of
 206 the ice (mainly due to H_2SO_4 and HNO_3), variable amounts of CaCO_3 are converted into soluble
 207 CaSO_4 and $\text{Ca}(\text{NO}_3)_2$ leading to a variable $\text{Ca}^{2+}/$ dust ratio (Legrand and Delmas, 1988). As an
 208 example, Fig. 2 shows the Ca^{2+} and mineral dust concentration of the NGRIP bag 3292 which
 209 we used to select the individual samples, and the relevant parameters measured for each sample
 210 of this bag. The data overview for all other measured NGRIP bags can be found in the Appendix
 211 A.



212
 213 **Figure 1: Overview of the analyzed NGRIP and GRIP samples over time.** All analyzed NGRIP and GRIP ice
 214 core samples are indicated on the NGRIP depth (m) on the bottom axis. To indicate an absolute age for the gas
 215 and ice records both the AICC2012 gas age (kyears BP) and the GICC05 ice age (kyears b2k) scale are provided
 216 on the upper axes. Note that for the purpose of describing the excess CH_4 production in a certain ice sample the
 217 age is irrelevant and we provide all records on depths throughout this manuscript. NGRIP samples measured from
 218 the five main bags (3292, 3331 & 3332, 3453, 3515) for the Keeling-plot approach are indicated with vertical lines
 219 in pink, NGRIP samples measured in 2011 and individual NGRIP ice core samples measured in 2019-2020 (not
 220 included in the Keeling-plot analyses) in turquoise, and GRIP ice core samples in green. **(a)** $[\text{CH}_4]$ record measured
 221 by wet extraction from NGRIP samples from Baumgartner et al. (2012, 2014). **(b)** $\delta^{18}\text{O}$ record from North
 222 Greenland Ice Core Project members (2004). **(c)** Ca^{2+} record from Erhardt et al. (2022).



224
225 Figure 2: **Detailed data overview for NGRIP bag 3292.** Bag-specific overview of several parameters measured
226 for each sample in this bag at a given depth: methane, ethane, propane, Ca^{2+} , mineral dust mass, TAC (Total Air
227 Content), $\delta^{13}\text{C-CH}_4$. At the top the AICC2012 gas age (upper top axis) and the GICC05 ice age (lower top axis) of
228 the respective depth are indicated. The mineral dust record is taken from Ruth et al. (2003), the Ca^{2+} record from
229 Erhardt et al. (2022). The data overview for all further measured NGRIP bags can be found in the Appendix A.

230

231

232 2.2 CH_4 , C_2H_6 , C_3H_8 and $\delta^{13}\text{C-CH}_4$ Analysis of Ice Core Samples

233

234 The short-chain alkanes and $\delta^{13}\text{C-CH}_4$ were measured at the University of Bern using the
235 discrete wet extraction technique as described in detail in Schmitt et al. (2014). With this
236 method it is possible to measure mixing ratios of methane, ethane, and propane as well as the
237 methane carbon isotopic signature and other trace gases on a single ice core sample of about
238 150 g.

239

240 Briefly, ice core samples are placed in a glass vessel locked by a stainless-steel flange which is
241 attached to the vacuum line to evacuate laboratory air (see Fig. 3, step a). Before melting the
242 ice sample, the leak tightness of the vacuum extraction line is tested with a so-called He blank.
243 The ice sample is then melted under vacuum with the help of infrared radiation for ~35 min to

244 release the enclosed air (step b). The released air is continuously removed from the sample
245 vessel by a pressure gradient towards an adsorbing AirTrap (activated carbon), collecting all
246 relevant air components at -180°C . After melting is completed, the temperature of the meltwater
247 is stabilized close to 0°C , but does not refreeze again. Afterwards, He is sparged with 4 mL/min
248 at standard temperature and pressure (equivalent to 100-400 mL at the varying low pressure in
249 the headspace) through the melt water for ~ 14 min through a capillary at the bottom of the
250 vessel to transfer any remnant gas species dissolved in the melt water onto the AirTrap (step c).
251 The sample vessel is then sealed by closing inlet and outlet valves (step d). Consecutively, the
252 AirTrap is warmed up in two steps to first remove N_2 and O_2 and in a second step to release the
253 gases of interest which are then sent after a cryofocus step to the gas chromatograph (GC) for
254 separation and quantification using an isotope ratio mass spectrometer (Isoprime 100,
255 Elementar).

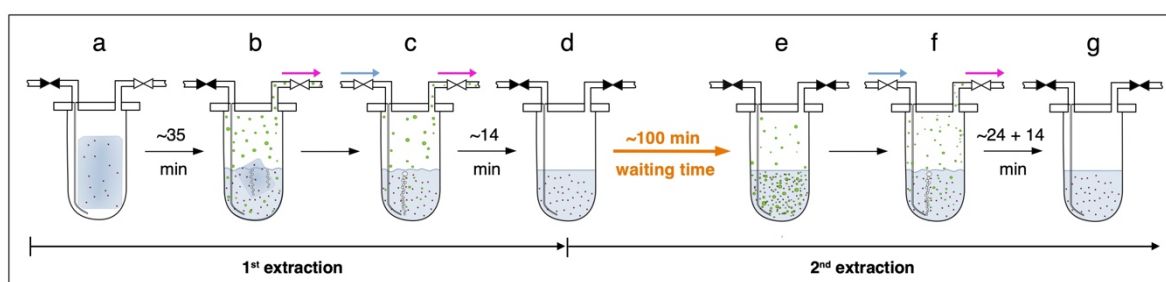
256
257 Precision of this method for CH_4 is about 8 ppb and 0.1 ‰ for $\delta^{13}\text{C}-\text{CH}_4$ based on the
258 reproducibility of the 1st extraction of ice core samples where isotopic data are expressed using
259 the δ notation on the international Vienna Pee Dee Belemnite (VPDB) scale. For C_2H_6 the
260 precision is 0.02 ppb or 1 ‰, for C_3H_8 0.03 ppb or 5 ‰ (whatever is higher) based on the
261 reproducibility of standard air samples which are by definition not subject to excess production
262 (Schmitt et al., 2014). Blank levels for these species based on melted artificial (gas-free) ice
263 samples are 1-2 ppb for CH_4 , 0.3 ppb for C_2H_6 and 0.2 ppb for C_3H_8 (Schmitt et al., 2014),
264 which are below the values measured on Antarctic ice, where excess production is minimal
265 compared to glacial Greenland samples (see Appendix B for details).

266
267 With their experimental investigations, Lee et al. (2020) were already able to demonstrate that
268 production/ release of $\text{CH}_{4(\text{xs})}$ is time dependent. We therefore conclude that this process does
269 not have to be completed in the time available for the gas extraction described above. We
270 continued the analyses of excess alkane production with an additional extraction step (here
271 referred to as 2nd extraction, steps d-g in Fig. 3) following the normal ice extraction routine.
272 After all sample air is collected in the 1st extraction, the meltwater is left in the isolated sample
273 vessel (the vessel is closed and not connected to the carbon trap) and held at temperatures close
274 to 0°C for ~ 100 min (step d). After this “waiting time” of ~ 100 min, He is purged through the
275 meltwater for ~ 24 min to extract the gases that have been accumulated during this time interval
276 simulating the extraction time of the 1st extraction, followed by another ~ 14 min of He purging
277 to mimic the last step of the ice extraction when the sample had completely melted (step f). The

278 gases from this 2nd extraction are collected and measured following the same trapping and
279 separation steps as in the 1st extraction. Note that the procedure of the 2nd extraction can be
280 repeated any number of times (e.g. 3rd extraction).

281
282 The amount of gases that we obtain from the 1st extraction comprises the atmospheric amount,
283 a possible contribution by in situ production, and a potential time-dependent production/release
284 in the meltwater (*in extractu*). The 2nd extraction, however, targets only the *in extractu* fraction.
285 The system blank for the 2nd extraction was estimated using the 2nd extraction of Antarctic ice
286 (Talos Dome, EDC) and were 2 ppb, 0.3 ppb and 0.3 ppb for CH₄, C₂H₆ and C₃H₈, respectively,
287 assuming an ice core sample air volume of 14 mL at standard temperature and pressure, which
288 is the typical ice sample size of 150 g with a total air content of 0.09 mL/g. For CH₄ this is <
289 1% of the amount of extracted species in the 1st extraction of glacial Greenland ice. Due to the
290 small amount of CH₄ analyzed in this 2nd extraction (about a factor of 20 to 50 less than for an
291 ice core sample) the precision for the $\delta^{13}\text{C}$ analysis is much lower than for the 1st (ice sample)
292 extraction and we estimate the precision of $\delta^{13}\text{C}\text{-CH}_4$ to 2 ‰ and for [CH₄] to be 2 ppb or 10
293 ‰ (based on the reproducibility of 2nd extractions of Antarctic EDC samples). For C₂H₆ and
294 C₃H₈, the precision is comparable to the 1st extraction. Note that throughout the manuscript we
295 do not perform blank corrections (neither for the measured alkane concentrations nor for the
296 isotopic values). The only exception is for the calculation of the temporal dynamics of excess
297 ethane production (see Appendix C) as the blank contribution would otherwise bias the samples
298 with low Ca²⁺ content.

299
300



301
302 **Figure 3: Sequential steps (a-g) happening in the ice core sample vessel during the 1st and the 2nd extraction**
303 **in the $\delta^{13}\text{C}\text{-CH}_4$ extraction line.** Scheme illustrates the subsequent steps as described in detail in the text.
304 Brownish spots indicate dust particles in the ice/ meltwater. Green circles indicate gas species (methane, ethane,
305 and propane) in the meltwater or in the headspace of the vessel. Closed valves are indicated in black, open valves
306 in white. Blue arrows indicate the He flow through the inlet capillary into the sample vessel, pink arrows indicate
307 the flow direction from the sample vessel towards the AirTrap.

308
309

310 **2.3 $\delta\text{D-CH}_4$ Analysis of Ice Core Samples**

311
312 All $\delta\text{D-CH}_4$ data presented here were measured at the University of Bern using the discrete wet
313 extraction technique as described in detail in Bock et al. (2010a, 2014). This $\delta\text{D-CH}_4$ device
314 allows to measure the concentration of methane and its deuterium isotopic signature ($\delta\text{D-CH}_4$)
315 on a single ice core sample of about 300 g.

316
317 Briefly, ice core samples are melted after evacuation of the headspace using a warm water bath
318 at 40°C for 25-30 min to release the enclosed air into the sample vessel headspace. Once all the
319 ice is melted, the warm water bath is replaced by an ice-water bath to keep the meltwater
320 temperature and water vapor pressure low but without refreezing. Note, in contrast to the $\delta^{13}\text{C-CH}_4$ -
321 CH_4 method, the inlet and outlet valves are closed during the melting process. The released air
322 leads to an increased pressure in the sample vessel headspace enhancing the solubility of gases
323 in water. After the melting is complete, the inlet and outlet valves are opened and He is purged
324 for ~40 min with a flow of 360 mL/min to transfer the accumulated air in the headspace and
325 bubble He through the meltwater to strip dissolved gases. Just like for the $\delta^{13}\text{C-CH}_4$ method,
326 the air is collected on an activated carbon trap followed by further purification steps including
327 GC separation. Note that compared to the $\delta^{13}\text{C-CH}_4$ device, we performed only one extraction
328 with the $\delta\text{D-CH}_4$ device.

329
330 For both methods, we assume that the time for an *in extractu* production during the ice
331 extraction procedure starts with the first presence of meltwater until He purging is stopped.
332 Note that this time is considerably longer for the $\delta\text{D-CH}_4$ analysis (~60 min) compared to the
333 time of the 1st extraction in the $\delta^{13}\text{C-CH}_4$ analysis (~35 min).

334
335 Using this method we can measure $[\text{CH}_4]$ and $\delta\text{D-CH}_4$ with a precision of about 15 ppb and 3
336 ‰ (based on standard ice sample measurements), where isotopic data are expressed using the
337 δ notation on the international Standard Mean Ocean Water (SMOW) scale.

338

339 **3. Characterization of excess alkanes in ice cores**

340 **3.1 Methane, ethane, propane concentrations**

341

342 As described in detail in Sect. 2.2 a full ice sample measurement includes the regular ice sample
343 extraction (1st extraction) and, after the waiting time of ~100 min, a 2nd gas extraction in the

344 meltwater. Gas from the 1st extraction is comprised of atmospheric air, a possible contribution
345 from in situ production, a potential time-dependent contribution by an *in extractu* process, and
346 any contribution from the device itself (blank). For the gas species discussed here (methane,
347 ethane, propane), these individual fractions are very different in magnitude. For polar ice core
348 samples, the atmospheric air is the major fraction of methane even in dust-rich, glacial ice from
349 Greenland prone to CH_{4(xS)} production (see below). The opposite is expected for ethane and
350 propane, which are dominated by the *in extractu* component in dust-rich Greenland ice. To
351 establish a better knowledge of alkanes in Greenland ice, we evaluated the measured
352 concentrations of methane, ethane, and propane, their ratios to each other and the relation to the
353 content of mineral dust in the ice for both the 1st and the 2nd extraction.

354

355 Note that different units to indicate concentrations of the trace gases of interest are used
356 throughout this study. By using mixing ratios in units of [ppb], as typically used for atmospheric
357 concentrations, the concentration of trace gases is related to the amount of air included in the
358 ice. Ice core samples with a low air content cause higher mixing ratio values for any additional
359 molecules produced in situ or *in extractu* compared to ice core samples with a high air content
360 and the interpretation might be biased. Alternatively, for any additional molecules produced in
361 situ or *in extractu*, [mol absolute per sample] denotes the absolute amount of trace gases and is
362 independent of the ice core air content. In the following, both units are used and great care has
363 to be taken to avoid misinterpretation of the results with respect to the different units.

364

365 **3.1.1 Excess alkanes in the 1st extraction**

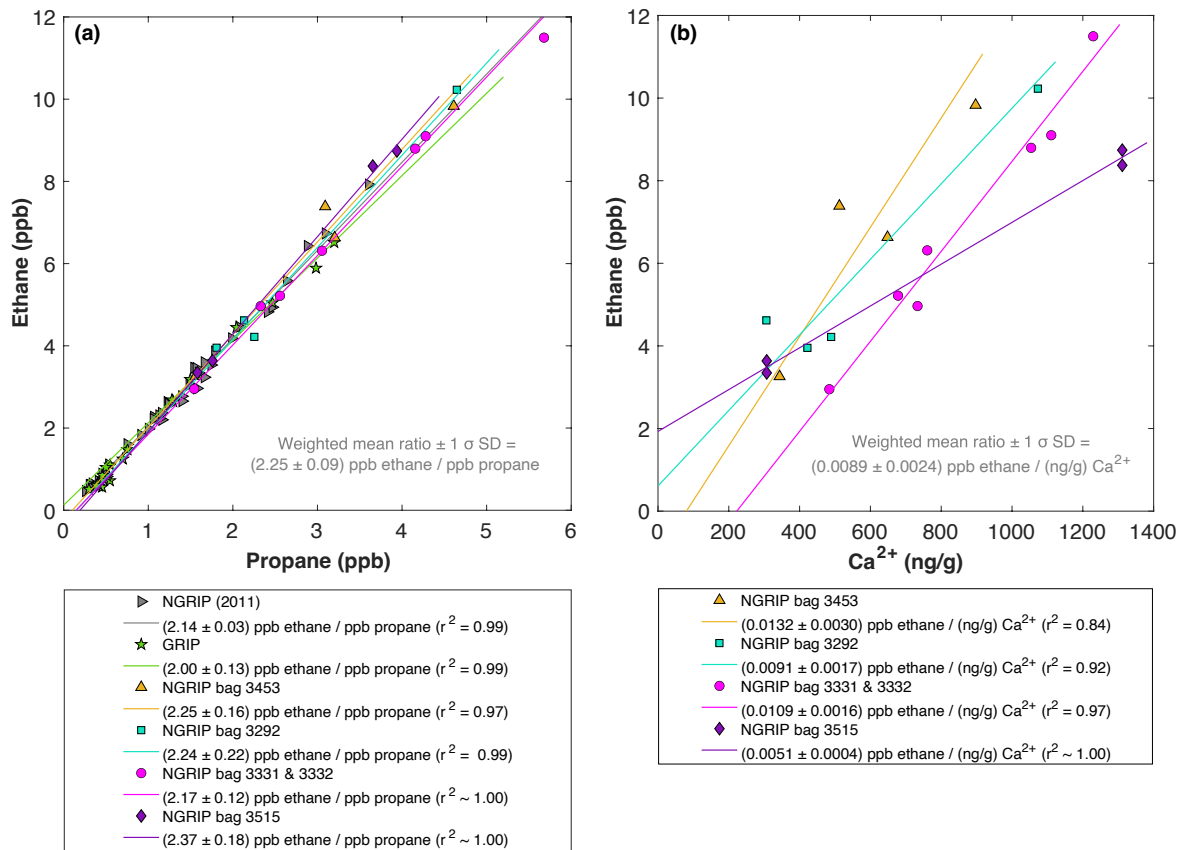
366

367 Figure 4 and 5 show results from the 1st extraction of our NGRIP and GRIP ice core samples.
368 For dust-rich samples, ethane ranges between 2 ppb and 12 ppb, and propane concentrations
369 between 1 ppb and 5 ppb. In contrast, low-dust samples from both GRIP and NGRIP have much
370 lower concentration (ca. 0.5 ppb for ethane, and 0.3 ppb for propane) consistent with estimates
371 of past atmospheric ethane and propane concentrations from the 15th to 19th century of the
372 common era being about 0.4 ppb in Greenland ice (Nicewonger et al., 2016) and lower for
373 propane (Helmig et al., 2013). Emissions of ethane and propane were likely reduced during the
374 glacial (Bock et al., 2017; Nicewonger et al., 2016; Dyonisius et al., 2020) thus, 0.5 ppb appears
375 to be an upper limit of past atmospheric concentrations of ethane and propane. This estimate of
376 past atmospheric ethane concentrations is an order of magnitude smaller than the values we
377 obtained from our dust-rich ice core samples from the 1st extraction, pointing to a strong

378 additional source of these alkanes for dust-rich samples. Thus, the unusually high mixing ratios
379 indicates that ethane and propane in glacial ice extracted using our melt technique on discrete
380 samples do not represent atmospheric levels.

381

382 As illustrated in Fig. 4 (left panel), the ethane and propane concentrations are highly correlated,
383 pointing to a common production of excess ethane and excess propane. The weighted mean
384 ratio and its weighted standard deviation (both weighted according to the number of samples
385 measured per bag) is (2.25 ± 0.09) ppb ethane/ ppb propane. Note that all regression lines are
386 calculated by following the method of York (1968) and York et al. (2004). York's analytical
387 solution to the best-fit line accounting for normally distributed errors both in x and y is widely
388 used to determine an isotopic mixing line and has been proven as the least biased method (Wehr
389 and Saleska, 2017; Hoheisel et al., 2019). Throughout the manuscript we use the 1 sigma (1σ)
390 standard deviation to express uncertainties. In Fig. 4, where the individual bags studied are
391 color-coded, we can clearly see that the ratio is essentially the same between the individual bags
392 and that the correlation is also very high within each bag (although we have to consider for the
393 significance of this correlation that the number of samples per bag is very low). This indicates
394 that for NGRIP ice ethane and propane are found in a fixed ratio. Accordingly, excess ethane
395 and propane production can be well represented by the weighted mean ratio and ethane and
396 propane are produced in a ratio of approximately 2:1. Very similar results were also observed
397 in NGRIP samples measured in 2011 and in GRIP samples revealing an ethane to propane ratio
398 of 2.14 ± 0.03 ($r^2 = 0.99$) and 2.00 ± 0.13 ($r^2 = 0.99$), respectively (see Fig. 4, left panel).



399

400 *Figure 4: NGRIP and GRIP results of ethane and propane from the 1st extraction. (a)* Concentrations of
 401 ethane and propane and their ratios to each other for NGRIP and GRIP samples measured in the 1st extraction of
 402 the $\delta^{13}\text{C}$ - CH_4 device. Colors and symbols indicate the different NGRIP bags or cores used. *(b)* Bag-specific
 403 production ratios of ethane in relation to the Ca^{2+} concentration for NGRIP samples. Note that for bag 3515 there
 404 is a data gap in the Ca^{2+} record and an anomaly of the Ca^{2+} to dust mass ratio for the replicate sample at 1932.7 m.
 405 Thus, the Ca^{2+} concentration for these two data points is likely overestimated (see Fig. A3).

406

407

408 Methane concentrations range from 407 ppb to 476 ppb and are predominantly of atmospheric
 409 origin (see Fig. 5). The amount of $\text{CH}_{4(\text{xs})}$ is the difference between the measured methane
 410 concentration and the atmospheric background concentration. To quantify $\text{CH}_{4(\text{xs})}$ we use the
 411 fact that due to the low-pass filtering of the bubble enclosure process all samples within one
 412 bag should have the same atmospheric CH_4 concentration. This also ensures that any physical
 413 processes that potentially influence the atmospheric alkanes in our samples (gravitational
 414 enrichment, thermodiffusion, disequilibrium effects on CH_4 isotopes) are the same for all
 415 samples within one bag. The only difference between these samples is, thus, the degree of
 416 $\text{CH}_{4(\text{xs})}$ production which can be estimated from the linear fit between the measured CH_4
 417 concentration and the concentration of another species (e.g. ethane, propane, mineral dust, or
 418 Ca^{2+}), which serves as a proxy for $\text{CH}_{4(\text{xs})}$ production. The closest relationship was found for
 419 $[\text{C}_2\text{H}_6]$ and quantifying $\text{CH}_{4(\text{xs})}$ was done by extrapolating the linear regression between ethane

420 and methane to an ethane concentration of 0.39 ppb, the assumed atmospheric [C₂H₆]. This
421 leads to an estimate of the true atmospheric [CH₄] value within the respective bag, a value that
422 can then be subtracted from the measured CH₄ concentration to obtain the CH_{4(x_s)} in each
423 sample. The uncertainty of the calculated CH_{4(x_s)} is typically 8 ppb.

424

425 Using the relation of ethane to methane this approach translates into CH_{4(x_s)} in the range of 14
426 ppb to 91 ppb for these five NGRIP bags with a mean excess of 39 ppb. Equivalent calculations
427 can be made using propane, dust, or Ca²⁺ as proxy for CH_{4(x_s)} production, however, the
428 relationship between dust parameters and CH_{4(x_s)} is more variable and does not lead to equally
429 precise values for CH_{4(x_s)}. Nevertheless, the obtained mean CH_{4(x_s)} using the relation of mineral
430 dust or Ca²⁺ to methane is similar in size to the one obtained by ethane.

431

432 We find that there exists a constant production ratio between all three excess alkanes for all
433 bags investigated. The weighted mean production ratio and its weighted standard deviation was
434 calculated to be (6.42 ± 1.57) ppb methane / ppb ethane and (14.3 ± 3.7) ppb methane/ ppb
435 propane for the samples of the five main NGRIP bags, and (2.25 ± 0.09) ppb ethane/ ppb
436 propane (also including NGRIP2011 and GRIP here). Note that there is a flagged sample for
437 CH₄ in bag 3453 (yellow asterisk in Fig. 5), where one vent (V6) was unintentionally open
438 during the measurement, which may have compromised the result. We therefore excluded the
439 production ratio determined from bag 3453.

440

441 In summary, we can characterize the excess alkane production in our measured NGRIP samples
442 by an overall methane/ethane/propane ratio of approximately 14:2:1. This constant relationship
443 between different alkanes suggests that excess alkanes are produced in a fixed ratio by a
444 common production process.

445

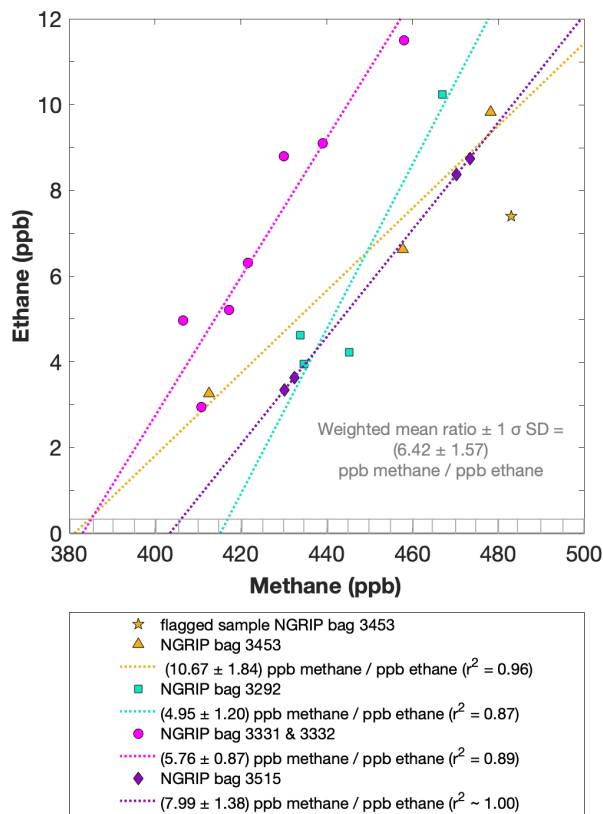
446 Another important observation is the close relation between excess alkanes and the content of
447 mineral dust within the ice core samples. Using measurements on GISP2 and NEEM ice core
448 samples, Lee et al. (2020) reported for the first time the close relation of CH_{4(x_s)} to chemical
449 impurities with the highest correlation with Ca²⁺. This is supported by our measurements on
450 NGRIP and GRIP samples revealing an overall increase of CH_{4(x_s)}, ethane, and propane with
451 increasing Ca²⁺ (see for example the ethane/Ca²⁺ relationship in Fig. 4, right panel). Although
452 the connection between ethane and Ca²⁺ is more variable than for ethane and propane between
453 the different bags, the slopes of the linear regressions in Fig. 4 (right panel) are still the same

454 within the 2 σ uncertainty and the weighted mean ratio of all NGRIP samples amounts to
 455 (0.0089 ± 0.0024) ppb ethane/ (ng/g) Ca^{2+} . However, this weighted mean value is likely biased
 456 low due to the relatively low ethane/ Ca^{2+} slope of bag 3515. Due to a data gap at 1932.7 m in
 457 the Ca^{2+} record, the corresponding Ca^{2+} concentration for two of the samples of this bag is
 458 subject to a large interpolation error and overestimated Ca^{2+} (see Fig. A3).

459
 460 The results agree with results from GRIP and older NGRIP (2011) samples, revealing an ethane/
 461 Ca^{2+} ratio of 0.0105 ± 0.0029 ($r^2 = 0.76$) and 0.0090 ± 0.0006 ($r^2 = 0.91$), respectively.

462 Based on the fixed ratio of excess CH_4 and ethane described above this translates into a
 463 weighted mean excess $\text{CH}_4/\text{Ca}^{2+}$ ratio of (0.0529 ± 0.0111) ppb methane per (ng/g) Ca^{2+} .

464



465
 466 **Figure 5: NGRIP results of methane and ethane from the 1st extraction.** Concentrations of methane (ppb) and
 467 ethane (ppb) and their ratios to each other for NGRIP samples measured in the 1st extraction of the $\delta^{13}\text{C}\text{-CH}_4$
 468 device. Different colors and symbols indicate the different NGRIP bags used for our analysis. Note that there is a
 469 flagged sample for CH_4 in bag 3453 as indicated with a yellow asterisk, which is not included in the ratio of bag
 470 3453. The grey hatched area indicates past atmospheric ethane concentrations of maximum 0.39 ppb as estimated
 471 by Nicewonger et al. (2016).

472

473

474

475 3.1.2 Excess alkanes in the 2nd extraction

476

477 With the 2nd extraction of the $\delta^{13}\text{C}$ -CH₄ analyses we can evaluate the temporal dynamics of
478 excess alkane production, assuming that all alkanes extracted in the 2nd extraction were
479 produced in the time after the 1st extraction was completed.

480 For our Greenland samples we measured a range of about 0.2 to 2.4 pmol for ethane and a range
481 of 0.1 to 1.2 pmol for propane in the 2nd extraction (Fig. 6, right panel). These values in pmol
482 are equivalent to 0.2 to 4.8 ppb of ethane and 0.2 to 2 ppb of propane assuming that the amount
483 of excess alkanes was added to 14 mL of ice core air (which is the typical ice sample size of
484 150 g with a total air content of 0.09 mL/g). The measured amount of methane ranges between
485 3 pmol and 20 pmol (Fig. 6, left panel).

486

487 The ratio of the measured amount for the individual species between the 1st and the 2nd
488 extraction amounts to 3.6 ± 0.85 ($r^2 = 0.78$) for ethane (Fig. 7, right panel), 3.3 ± 0.33 ($r^2 =$
489 0.78) for propane (combined data of NGRIP and GRIP) and 3.8 ± 1.62 ($r^2 = 0.33$) for methane
490 (only NGRIP data), where the uncertainty for CH₄ is again much larger. Thus, we can conclude
491 that the amount of alkanes produced during the waiting time after the 1st extraction until the 2nd
492 extraction was finished, was approximately 30% of the amount produced during the 1st
493 extraction. Results from the 2nd extraction also demonstrate that this process is slow and not
494 completed during the time of the 1st extraction. We can thereby confirm the results of Lee et al.
495 (2020) but we are able to show for the first time that this process leads also to production of
496 excess ethane and propane.

497

498 For a better estimate of the temporal reaction kinetics of the underlying process, we can relate
499 the measured amount of the individual species to the time available for a potential reaction in
500 the meltwater during each extraction. For the five GRIP samples that were measured with a 2nd
501 and 3rd extraction (see Sec. 2.2 for details) we take the cumulative production amount (where
502 the first data point is the produced amount in the 1st extraction, the second data point is the sum
503 of the 1st and 2nd extraction, and the third data point is the sum of the 1st, 2nd, and 3rd extraction).
504 In the example shown for ethane (Fig. C1, Appendix C) we can see the assumed first-order
505 reaction kinetics with a saturation of ethane accumulation over time providing a good model
506 for our measurements (details on the calculation can be found in the Appendix C). With that,
507 we can estimate the half-life time (τ) of the production to be approximately 30 min. Note that
508 this long half life has also an implication for a potential excess production of CH₄ in continuous

509 flow techniques, where the reaction time before the air is separated from the liquid water stream
510 is only 1-2 min. Thus, only 5-10 % of the *in extractu* production found in our 1st extraction can
511 be expected in such continuous flow measurements, which are difficult to detect.

512
513 The goodness of fit of the ratios of the measured concentrations between the 1st and the 2nd
514 extraction is $r^2 = 0.78$ for both ethane and propane, indicating that the production/release in the
515 1st extraction in relation to the 2nd extraction is well correlated for both species (see Fig. 7b for
516 ethane). Thus, samples that produced higher excess alkanes during the 1st extraction also
517 produced more excess alkanes in the 2nd extraction, suggesting that the production is dependent
518 on the amount of some reactant present in the samples from which excess alkanes are produced.
519 Again, for CH₄ this relationship is more variable which is likely related to the higher uncertainty
520 in measuring CH₄ for the 2nd extraction.

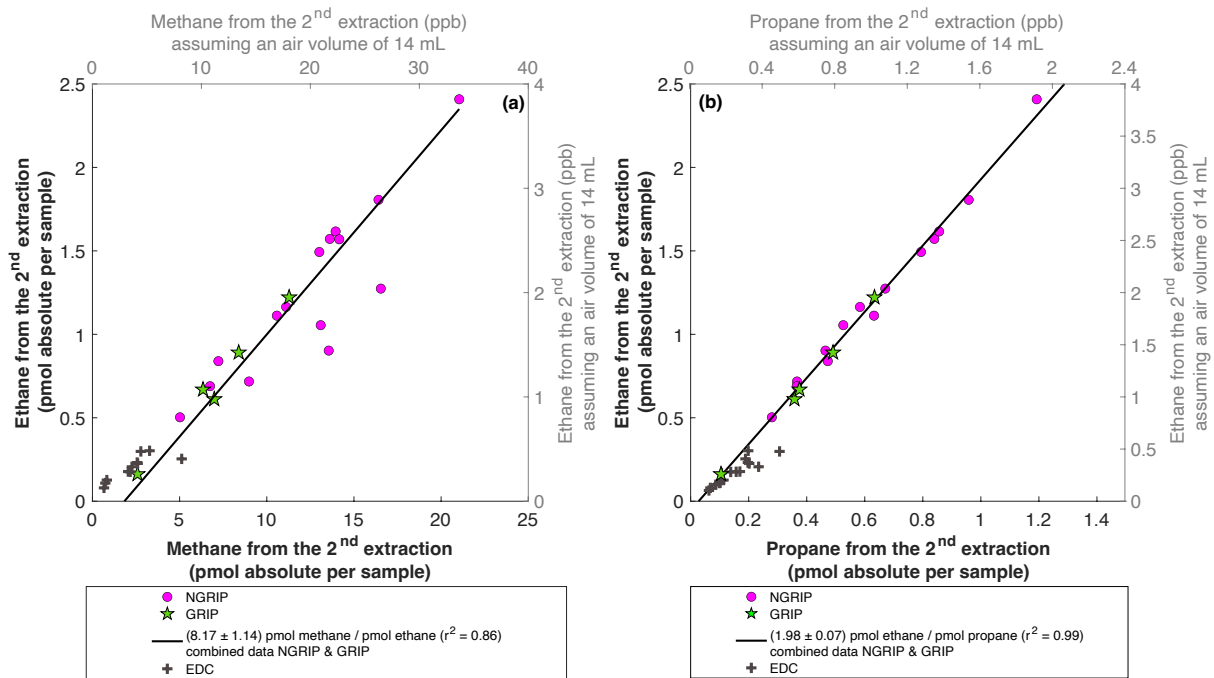
521
522 The ratio of ethane to propane of all measured Greenland samples in the 2nd extraction is 1.98
523 ± 0.07 ($r^2 = 0.99$). The ratio of methane to ethane is 8.17 ± 1.14 ($r^2 = 0.86$). Accordingly, the
524 overall relationship between methane, ethane, and propane in the 2nd extraction can be
525 characterized by a ratio of approximately 16:2:1. However, comparing the ratios of
526 ethane/propane and methane/ethane between the 1st and the 2nd extraction, there is no significant
527 difference within the 2σ uncertainties from 2.25 ± 0.09 to 1.98 ± 0.07 , and from 6.42 ± 1.57 to
528 8.17 ± 1.14 . We can conclude that within the error limits, the production ratios stayed the same,
529 suggesting that the same *in extractu* process is at play during both extractions.

530
531 In the 2nd extraction, we can again observe the relation between excess alkanes and the amount
532 of mineral dust. Figure 7a shows the correlation of ethane (fmol/g meltwater) to Ca²⁺ (ng/g) in
533 all measured NGRIP and GRIP samples in the 2nd extraction revealing a production of $(0.0085$
534 $\pm 0.0011)$ fmol/(g meltwater) ethane per (ng/g) Ca²⁺ with $r^2 = 0.70$. For methane, we observe a
535 production ratio of (0.0556 ± 0.01513) fmol/(g meltwater) methane per (ng/g) Ca²⁺ with a
536 correlation of $r^2 = 0.47$ (data not shown).

537
538 Overall, excess alkane concentrations are increasing with increasing Ca²⁺ concentrations, in
539 both the 1st and the 2nd extraction. The total alkane production/release, however, decreased in
540 the 2nd extraction, suggesting the progressive exhaustion over time of some reactant necessary
541 for the *in extractu* process. We propose that this reactant co-varies with Ca²⁺ and particulate

542 dust, where Ca^{2+} is of course not a reactant itself and represents only a proxy for higher *in*
543 *extractu* production.

544



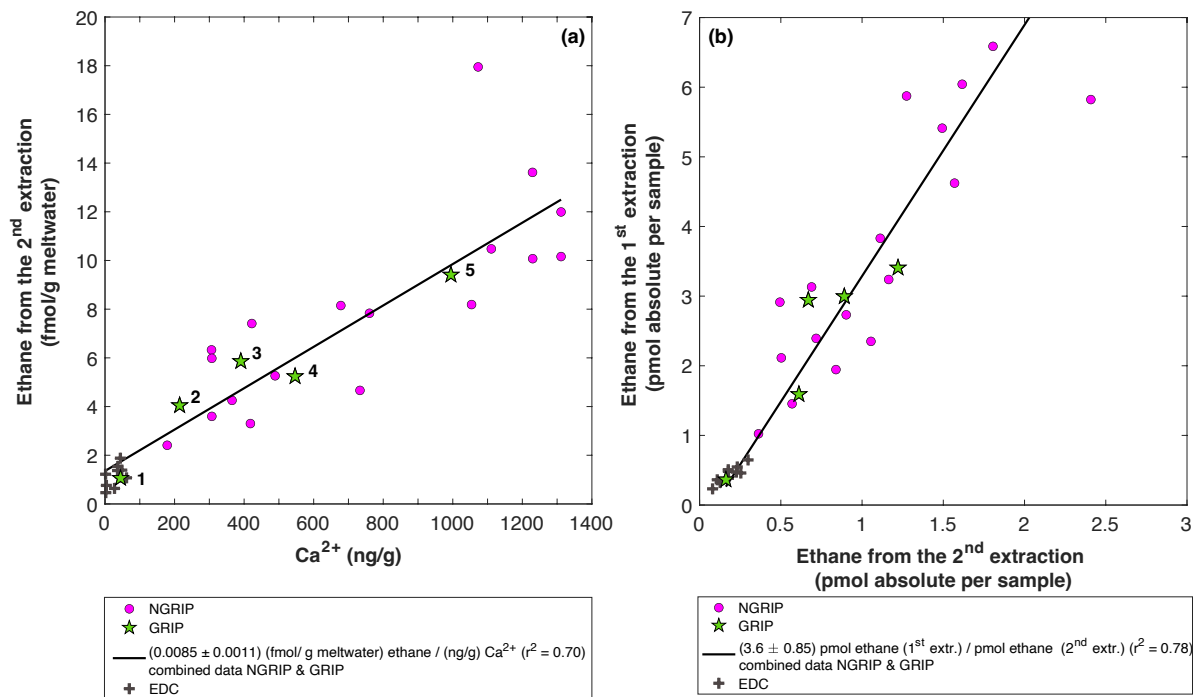
545

546 **Figure 6: NGRIP and GRIP results of excess methane, ethane, and propane from the 2nd extraction. (a)**
547 **Concentrations of methane and ethane and their ratios to each other. (b) Concentrations of propane and ethane and**
548 **their ratios to each other. Units are given as pmol absolute per sample on the primary axis in black and in ppb**
549 **assuming an air volume of 14 mL of the ice core sample on the secondary axis in grey. Grey crosses indicate the**
550 **blank level of the system estimated from 2nd extractions of EDC ice core samples.**

551

552

553



554
555

556 **Figure 7: GRIP and GRIP results of ethane from the 2nd extraction in relation to the Ca²⁺ concentration**
 557 **and to the 1st extraction. (a)** Produced amount of ethane in the meltwater (fmol/g meltwater) in relation to the
 558 Ca²⁺ concentration in the ice core samples. The numbered GRIP samples are used in Figure C1 to evaluate the
 559 temporal dynamics. Grey crosses indicate the blank level of the system estimated from 2nd extractions of EDC
 560 ice core samples. **(b)** Relation of the amount of ethane (pmol) measured in the 1st and 2nd extraction.

561
562
563

3.2 Isotopic composition of excess methane

564 In this section we characterize the isotopic signature of excess methane and explore how we
 565 can use this parameter to better identify its source or production pathway. The evaluation of the
 566 carbon and deuterium isotopic signature of excess methane ($\delta^{13}\text{C-CH}_4(\text{xs})$ and $\delta\text{D-CH}_4(\text{xs})$) is
 567 based on the Keeling-plot approach (Keeling, 1958, 1961; Köhler et al., 2006).

568

3.2.1 $\delta^{13}\text{C-CH}_4$ isotopic signature of excess methane

570

571 Figure 8 (left panel) shows the $\delta^{13}\text{C-CH}_4$ results of the 1st extraction. The carbon isotopic
 572 signature of excess CH₄ from the 1st extraction of the ice core sample measurements within one
 573 NGRIP bag are obtained from the y-intercept of the Keeling-plot, representing the excess $\delta^{13}\text{C-CH}_4$
 574 value for this bag. Note that the two NGRIP bags 3331 and 3332 are neighbouring bags
 575 and were therefore combined into one Keeling y-intercept. As the individual samples in these
 576 two bags span less than 10 years between each other, they are the same within the age
 577 distribution, and the assumptions for the Keeling-plot approach (see Sec. 2.1) are met. All bags
 578 show agreement in $\delta^{13}\text{C-CH}_4$ signature (y-intercepts) within 2 σ uncertainties. The weighted

579 mean isotopic signature is $(-47.0 \pm 2.9) \text{ ‰}$, with weights assigned by the number of samples
580 that constrained each individual Keeling plot regression line.

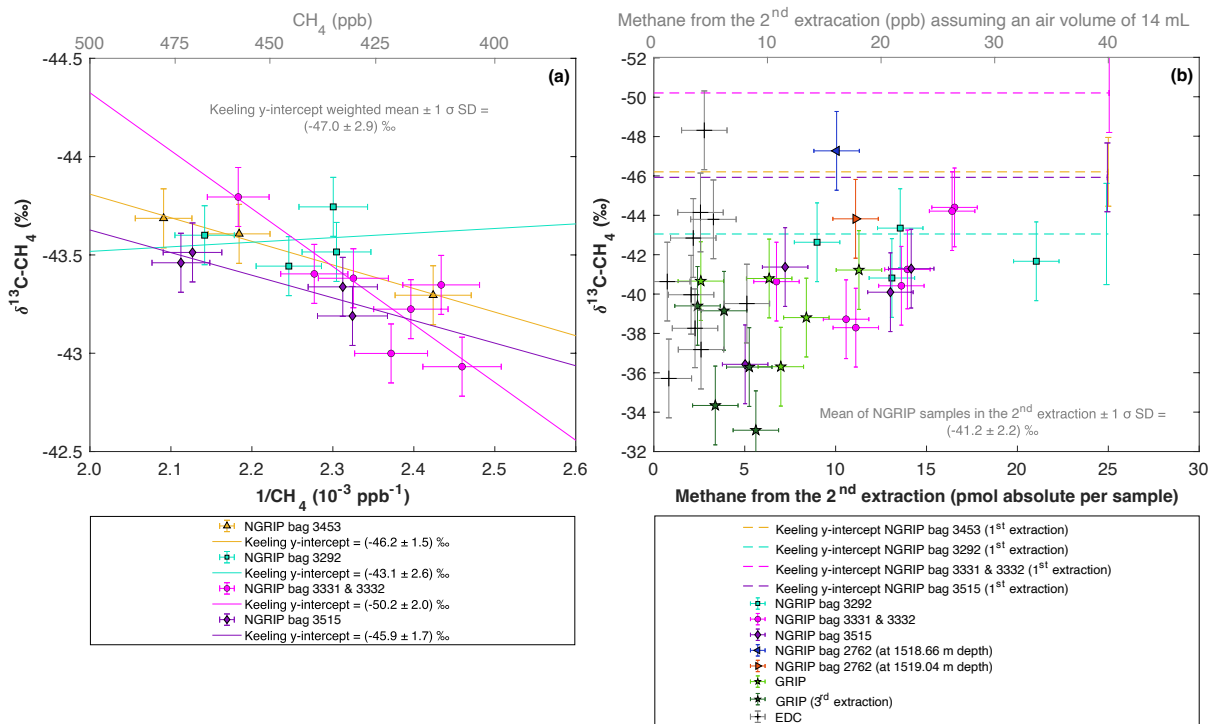
581
582 Figure 8 (right panel) shows the isotopic results in relation to the amount of CH_4 produced
583 during the 2nd extraction. No atmospheric CH_4 is present during the 2nd extraction and the
584 individual isotopic values in Fig. 8 (right panel) are the directly measured values of excess CH_4
585 without applying the Keeling-plot approach. For a better comparison, the produced CH_4 is
586 shown both in pmol (lower axis in Fig. 8, right panel) and in a mixing ratio CH_4 scale (ppb).
587 The Keeling y-intercept values of the 1st extraction are added in the right panel of Fig. 8.

588
589 The $\delta^{13}\text{C}-\text{CH}_4$ values of the 2nd extraction range between -34 ‰ and -48 ‰ with the mean being
590 $(-41.2 \pm 2.2) \text{ ‰}$. This value appears isotopically somewhat heavier compared to the weighted
591 mean of $(-47.0 \pm 2.9) \text{ ‰}$ inferred from the Keeling analysis, however, is still the same within
592 the 2σ error limits. We note that the measured peak areas for the 2nd extractions are very small
593 and lie outside of the typical range of our gas chromatography mass spectrometry analysis for
594 $\delta^{13}\text{C}-\text{CH}_4$ and we cannot exclude some bias in these results. However, we mimicked these small
595 peak areas with injections of small amounts of standard air and observed no significant bias in
596 the measured $\delta^{13}\text{C}-\text{CH}_4$ values given that the precision of such small peaks is around 2 ‰ .

597
598 Another caveat is the considerable blank contribution for CH_4 that we observe for the 2nd
599 extraction. Since Antarctic ice cores do not show a sizable *in extractu* production (Fig. 7, grey
600 crosses for EDC) we measured EDC samples with the same protocol of a 2nd extraction as for
601 our Greenland samples to provide an upper boundary of this blank. Hence the 2nd extraction of
602 the EDC samples are a conservative blank estimate while the true system blank is lower. As
603 can be seen in Fig. 8 (right panel) the amount of CH_4 measured for these EDC samples (grey
604 crosses) is on average about 2 pmol (equivalent to about 3 ppb). For comparison, our ice
605 samples from Greenland show a range of about 5 to 20 pmol, indicating a considerable blank
606 contribution in the 2nd extraction.

607
608 To estimate the influence of the blank on the isotopic signature that occurs during the 2nd
609 extraction we used the values from our EDC measurements and applied an isotope mass balance
610 approach. The $\delta^{13}\text{C}-\text{CH}_4$ blank signature obtained from these EDC samples is -39.0 ‰ , hence
611 a few ‰ heavier than the mean $\delta^{13}\text{C}-\text{CH}_4$ signature of the excess CH_4 from this 2nd extraction
612 for the Greenland samples. On average, the correction would shift our NGRIP values towards

613 lighter (more negative) values by 0.31 ‰. This systematic correction is thus small compared to
 614 the typical measurement precision obtained both from the Keeling-plot approach and the direct
 615 measurement of the CH_{4(xS)} with the 2nd extraction. As the δ¹³C-CH₄ signature of the blank is
 616 close to the NGRIP values, performing a blank correction has only little leverage. Considering
 617 these analytical limitations of our 2nd extraction for δ¹³C-CH₄, these findings suggest that
 618 CH_{4(xS)} produced during the 1st and 2nd extraction has the same δ¹³C-CH₄ isotopic signature
 619 within the 2 σ error limits and is likely produced/released by the same process in both
 620 extractions.
 621



622
 623 **Figure 8: NGRIP (and GRIP) δ¹³C-CH₄ results of the 1st and 2nd extraction measured with the δ¹³C-CH₄**
 624 **device. (a) Keeling-plot of δ¹³C-CH₄ for NGRIP samples from the five main bags (3292, 3331 & 3332, 3453,**
 625 **3515) measured in the 1st extraction. Colors and symbols indicate individual measurements of the respective bags.**
 626 **Colored lines indicate the corresponding Keeling regression line of each individual bag. (b) δ¹³C-CH₄ (‰)**
 627 **values in relation to the amount of methane measured for the 2nd extraction. Units for CH₄ are given as pmol absolute per**
 628 **sample on the primary axis in black, and in ppb assuming an air volume of 14mL of an ice core sample on the**
 629 **secondary axis in grey. Colors and symbols indicate individual measurements of the respective bags. Color-coded**
 630 **lines indicate the corresponding Keeling y-intercept of each individual bag as measured in the 1st extraction. Grey**
 631 **crosses indicate the blank level of the system estimated from 2nd extractions of EDC ice core samples.**

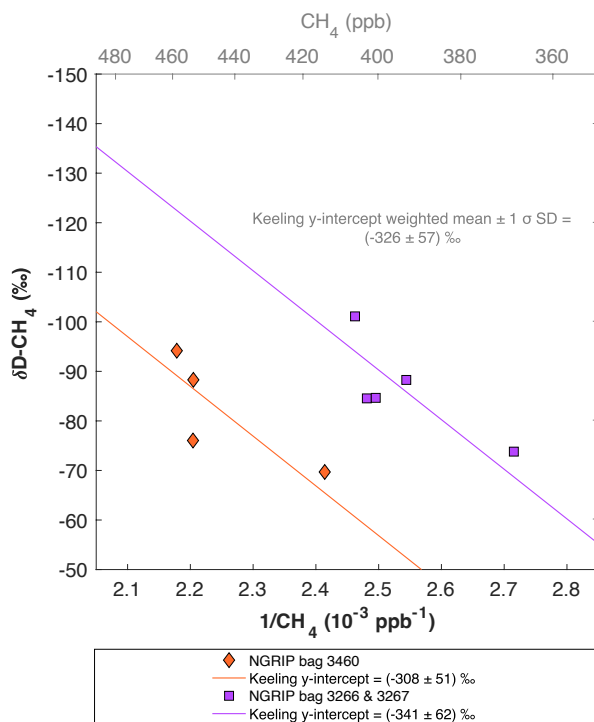
632
 633 **3.2.2 δD-CH₄ isotopic signature of excess methane**

634
 635 Figure 9 shows the isotopic results of the δD-CH₄ analyses. Due to the larger sample size
 636 required for the δD-CH₄ analyses and the sample availability restrictions only two bags could
 637 be studied for δD-CH₄. The individual isotopic results obtained from the ice core sample

638 measurements within one NGRIP bag are again combined into one Keeling y-intercept,
 639 representing the $\delta\text{D-CH}_4$ value for this bag. NGRIP bag 3460 (orange) reveals a Keeling y-
 640 intercept $\delta\text{D-CH}_4$ value of $(-308 \pm 51) \text{‰}$. The two NGRIP bags 3266 and 3267 (purple)
 641 neighbouring bags and were therefore combined into one Keeling y-intercept revealing a $\delta\text{D-}$
 642 CH_4 value of $(-341 \pm 62) \text{‰}$. The difference between the two Keeling y-intercepts of the
 643 individual bags is within the error limits. Accordingly, we combine the two values to a weighted
 644 mean and weighted uncertainty of $(-326 \pm 57) \text{‰}$.

645 Our results are consistent with the findings of Lee et al. (2020), who used the NGRIP $\delta\text{D-CH}_4$
 646 record of Bock et al. (2010b) and the NGRIP $[\text{CH}_4]$ record of Baumgartner et al. (2014) to
 647 estimate the $\delta\text{D-CH}_{4(\text{xs})}$ signature in these samples. Assuming a two-component mixture of
 648 atmospheric methane and excess methane in their model led to a best estimate of (-293 ± 31)
 649 ‰ for $\delta\text{D-CH}_{4(\text{xs})}$ which is within the error limits of our Keeling-plot results.

650



651

652 **Figure 9: NGRIP $\delta\text{D-CH}_4$ results.** Keeling-plot of $\delta\text{D-CH}_4$ of NGRIP samples measured with the $\delta\text{D-CH}_4$ device.
 653 Colors and symbols indicate individual measurements of the respective bags and colored lines indicate the
 654 corresponding regression of each individual bag.

655

656 4. Testing the hypotheses explaining excess alkanes

657

658 In Sect. 3 several pieces of evidence for the production/release of excess alkanes in Greenland
 659 ice core samples were collected:

660

- 661 - We can confirm the observations of Lee et al. (2020) on excess methane in different
662 Greenland ice cores and its covariance with the amount of mineral dust in the ice.
663 Despite the different extraction techniques applied (multiple melt-refreeze method in
664 Lee et al. (2020) versus two subsequent wet extractions in our study), we can further
665 corroborate that the temporal dynamics of the production/release is on the order of hours
666 and production/ release occurs when liquid water is present during extraction.
- 667 - We document for the first time a co-production/release of excess methane, ethane, and
668 propane, with the observed values for ethane and propane exceeding by far their
669 estimated past atmospheric background concentrations.
- 670 - Excess alkanes (methane, ethane, propane) are produced/ released in a fixed molar ratio
671 of approximately 14:2:1, indicating a common origin.
- 672 - We further characterize the isotopic composition of excess CH₄ of $\delta^{13}\text{C-CH}_{4(\text{xs})}$ and $\delta\text{D-}$
673 $\text{CH}_{4(\text{xs})}$ to be $(-47.0 \pm 2.9) \text{‰}$ and $(-326 \pm 57) \text{‰}$ in NGRIP ice core samples,
674 respectively. Within the error limits, our $\delta\text{D-CH}_{4(\text{xs})}$ results are consistent with the
675 calculated best estimate of $(-293 \pm 31) \text{‰}$ by Lee et al. (2020).

676

677 In the introduction we presented the hypotheses proposed by Lee et al. (2020) explaining their
678 observations on CH_{4(xs)}. Here we resume the discussion of the original hypotheses and refine
679 them in light of our new data from NGRIP and GRIP ice sample measurements. An overview
680 of the different possible sources explaining excess alkanes is illustrated in Fig. 10 and Table 1.
681 We discuss in the following three options for the origin of the observed excess alkanes:

682

683 1.) Excess alkanes could be adsorbed on mineral dust particles prior to their deposition on the
684 Greenland ice sheet and released in the laboratory during the prolonged melting process. The
685 adsorption step could happen in the mineral dust source region (East Asian deserts) thereby
686 adsorbing the alkanes from natural gas seeps within the sediment (process marked as A1, see
687 Fig. 10). Alternatively, adsorption of atmospheric alkanes on dust particles can happen anytime
688 starting from the soil surface in the dust source region, during atmospheric transport to the
689 Greenland ice sheet after deflation, or within the firn layer before pores are closed-off (A2).
690 The desorption of the adsorbed alkanes happens during the melting process for both cases.

691

692 2.) Excess alkanes could be produced microbially. The production happens either in the ice
693 itself (in situ), the alkanes are adsorbed on dust particles in the ice and then slowly released

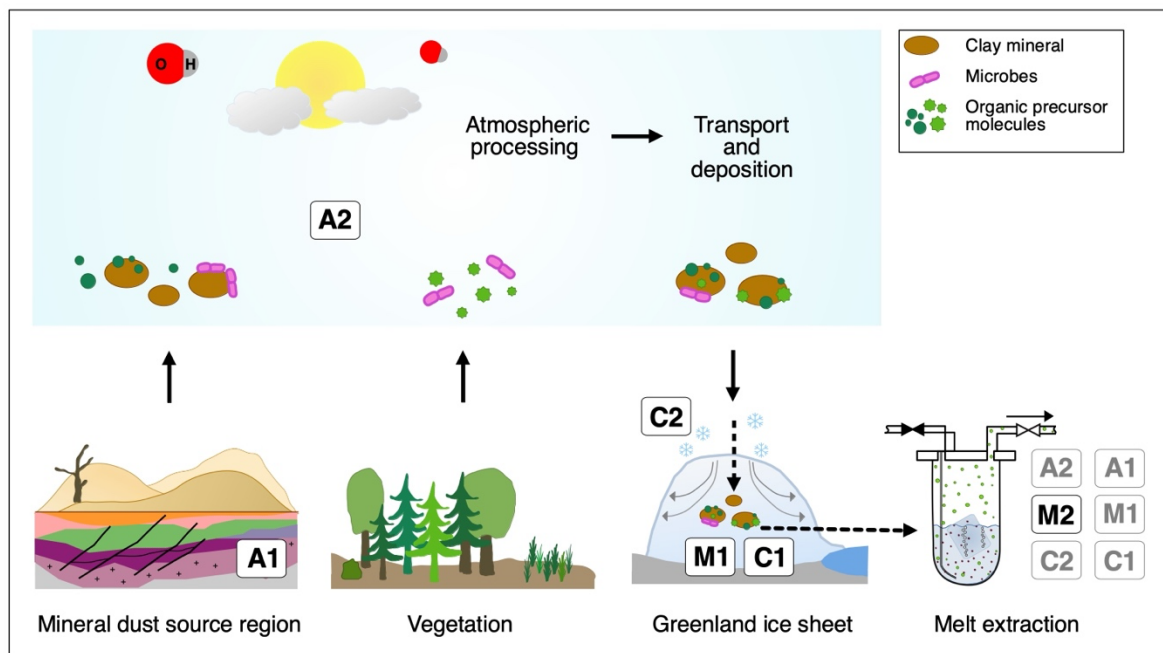
694 during the melting phase in the laboratory (M1). Alternatively, the microbial production
 695 happens in the meltwater during the melting process (*in extractu*) (M2). A microbial in situ
 696 production in the ice without an adsorption-desorption process was already deemed unlikely by
 697 Lee et al. (2020) since it is not compatible with the lack of excess CH₄ in the CFA CH₄
 698 concentration records.

699 3.) Excess alkanes are produced abiotically, e.g. by the decomposition of labile organic
 700 compounds. This chemical reaction can happen either in the ice itself (in situ), where excess
 701 alkanes are then adsorbed on dust particles and subsequently released during the melting
 702 process (C1), or in the meltwater during extraction (*in extractu*) (C2). An abiotic in situ
 703 production in the ice without an adsorption-desorption process can also be ruled out with the
 704 CFA evidence.

705

706 We now discuss these mechanisms in detail and evaluate the viability of the different
 707 hypotheses in the light of our new experimental observations.

708



709

710 **Figure 10: Overview of the different possibilities explaining excess alkanes in dust-rich Greenland ice.** A
 711 depicts an adsorption process of alkanes on mineral particles, either from natural gas seeps within the sediment
 712 (A1) or from the atmosphere (A2) prior to their deposition on the Greenland ice sheet. This gas is then desorbed
 713 during the melting process in the laboratory. **M** depicts a microbial production of excess alkanes, either in the ice
 714 itself (in situ), followed by adsorption on dust particles in the ice and a subsequent slow desorption process during
 715 the melting process (M1), or a microbial production in the meltwater (*in extractu*) (M2). **C** depicts the abiotic/
 716 chemical production of excess alkanes, either in the ice itself (in situ) followed by adsorption on dust particles
 717 after production in the ice and a subsequent slow desorption during the melting process (C1), or abiotic production
 718 in the meltwater (*in extractu*) (C2).

719

720

721 **(1) Adsorption/desorption of alkanes on mineral dust particles**

722 Depending on where the adsorption takes place, the mineral particles might adsorb alkanes of
723 different origin and composition. One possibility is that the adsorption already takes place
724 within the sediment or soil of the dust source region, thus before mineral dust deflation (erosion
725 of loose material by winds from flat and dry areas; A1). As proposed by Lee et al. (2020), the
726 major source region of mineral dust arriving in Greenland during the glacial (Taklamakan,
727 Tarim Basin) are also regions where natural gas seeps reach the surface (Etiope and Klusman,
728 2002; Etiope et al., 2008). In this case the methane should reflect the isotopic composition and
729 alkane composition of the seep. Alternatively, adsorption of atmospheric alkanes on the
730 particles can happen anytime starting from the soil surface, during transport en route to the
731 Greenland ice sheet after deflation and within the firn layer before pores are closed-off (A2).
732 For the scenario A2 the fingerprint (isotopic composition and ratio of alkanes) of the adsorbed
733 alkanes depends on the past atmospheric composition but could be modulated by selective
734 fractionation processes during adsorption and desorption.

735

736 To be a viable mechanism for our problem, it requires that the adsorbed alkanes stay strongly
737 bound at the mineral dust particles while desorption is minor both during the atmospheric
738 transport and during the several hundred years the dust particle spends in the porous firn (age
739 of the firn at bubble close-off). During the melting procedure the adsorbed alkanes would then
740 be released from their mineral dust carrier, which in case of Greenland ice from glacial times
741 is predominately consisting of clay minerals from the Taklamakan (and partly also Gobi) desert
742 (Biscaye et al., 1997; Svensson et al., 2000; Ruth et al., 2003). However, other additional dust
743 sources exist with their relative contribution varying with climate conditions (Han et al., 2018;
744 Lupker et al., 2010).

745

746 Several experimental studies showed that clay minerals have a high adsorption capacity and
747 retention potential for alkanes (Sugimoto et al., 2003; Cheng and Huang, 2004; Dan et al., 2004;
748 Pires et al., 2008; Ross and Bustin, 2009; Ji et al., 2012; Liu et al., 2013; Tian et al., 2017).
749 Influencing parameters for an adsorption-desorption process are mainly pressure, temperature,
750 clay mineral type, micropore size, surface area, organic carbon content, and water/ moisture
751 content (Sugimoto et al., 2003; Cheng and Huang, 2004; Dan et al., 2004; Pires et al., 2008;
752 Ross and Bustin, 2009; Ji et al., 2012; Liu et al., 2013; Tian et al., 2017). Most interestingly for
753 us, studies by Sugimoto et al. (2003) and Dan et al. (2004) on the adsorption of CH₄ in
754 micropores on the surface of clay minerals in dried and fresh lake sediment showed that dried

755 sediment still retains CH₄ and that dried and degassed sediment re-adsorbs ambient CH₄ at
756 standard pressure and room temperature. The amount of CH₄ adsorbed in their samples is
757 strongly dependent on pressure and temperature while increasing temperatures and decreasing
758 pressure lead to a stronger desorption. The addition of water/ moisture leads to a rapid
759 desorption of already adsorbed gases (Sugimoto et al., 2003; Dan et al., 2004; Pires et al., 2008;
760 Ji et al., 2012; Liu et al., 2013).

761
762 These results in principle support the possibility of an adsorption-desorption process for our
763 glacial NGRIP and GRIP ice core samples, where alkanes (from fossil seeps or atmosphere)
764 would be adsorbed on dust particles and desorbed during the measurement procedure when
765 liquid water is present. Independent of the origin of the alkanes (A1 or A2) the amount of
766 alkanes deposited onto the Greenland ice sheet by this process would be diminished if mineral
767 dust particles were already in contact with liquid water during the long-range transport which
768 may lead to a loss of previously adsorbed alkanes already in the atmosphere. This water contact
769 could occur for example already at the dust source, as it is known that the deserts in the Tarim
770 basin receive regular input from water from the surrounding mountain regions also providing
771 the minerals to the basin that are blown out of the desert afterwards (Ruth et al., 2007).

772
773 To explain the constant ratio of methane, ethane, and propane of 14:2:1 in our samples with an
774 adsorption mechanism, we need to discuss the potential origins of the adsorbed alkanes. First,
775 we find very high relative excess contributions of ethane and propane in our samples, while we
776 see a small excess contribution for methane compared to the atmospheric background. If we
777 assume a comparable adsorption for all three alkanes, this would imply a strong relative
778 enrichment of ethane and propane over methane in the concentration of these gases during
779 adsorption. This is not in line with the past atmospheric CH₄/(C₂H₆+C₃H₈) ratio where past
780 atmospheric ethane concentrations by Nicewonger et al. (2016) are an order of magnitude
781 smaller (and propane concentrations even less) than the measured concentrations in our NGRIP
782 and GRIP ice core samples.

783 In contrast, the ratio of methane, ethane, and propane for our samples of approximately 14:2:1,
784 translates into a CH₄/(C₂H₆+C₃H₈) ratio of ~5, which is most consistent with a thermogenic
785 origin (see Fig. 11, left panel). However, due to the different adsorption capacity of mineral
786 dust particles, also a fractionation of the three alkanes is to be expected during the adsorption
787 process, which could alter the thermogenic signature-

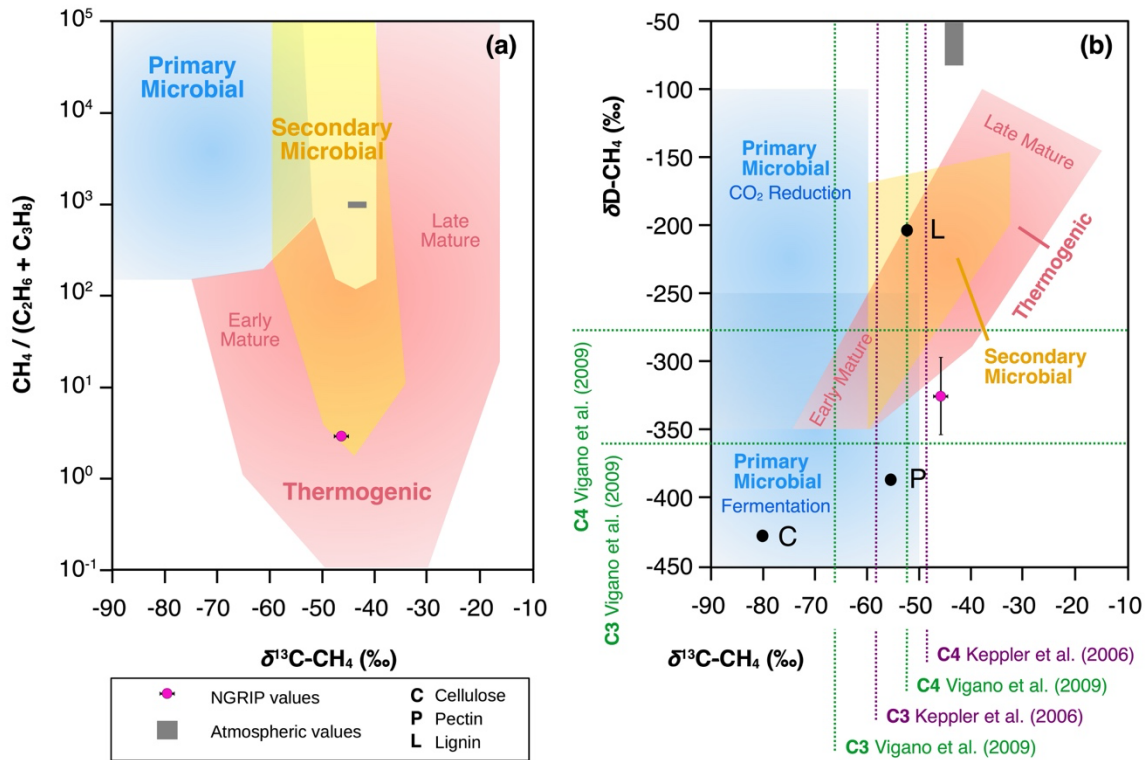
788

789 To further evaluate the adsorption theory in the light of our experimental evidence, we now
790 include the carbon and deuterium isotopic signature of $\text{CH}_{4(\text{xs})}$ in our samples. Our NGRIP
791 samples reveal a $\delta^{13}\text{C}-\text{CH}_{4(\text{xs})}$ value (Keeling y-intercept weighted mean) of $(-47.0 \pm 2.9) \text{‰}$
792 which is within the error consistent with contemporaneous atmospheric values or with
793 emissions from seeping reservoirs of natural gas. In contrast, our hydrogen isotopic
794 measurements on NGRIP samples reveal a very light $\delta\text{D}-\text{CH}_{4(\text{xs})}$ value (Keeling y-intercept
795 weighted mean) of $(-326 \pm 57) \text{‰}$ and slightly outside of the field of a thermogenic origin (see
796 Fig. 11). The value is similar to the estimate by Lee et al. (2020), which, however, lies inside
797 the field of a thermogenic origin (see Fig. 11). While both the low $\text{CH}_4/(\text{C}_2\text{H}_6+\text{C}_3\text{H}_8)$ ratio and
798 the $\delta^{13}\text{C}-\text{CH}_{4(\text{xs})}$ could be indicative of a thermogenic source (A1), the light $\delta\text{D}-\text{CH}_{4(\text{xs})}$ signature
799 is far away from the atmospheric $\delta\text{D}-\text{CH}_4$ value and is borderline in line with typical $\delta\text{D}-\text{CH}_4$
800 values of a thermogenic origin. Hence, our $\delta\text{D}-\text{CH}_{4(\text{xs})}$ values exclude the atmospheric
801 adsorption scenario A2 and put a question mark after the seep adsorption scenario A1.

802

803 For the seep adsorption scenario A1 to work the dust particles on which the thermogenic gas
804 adsorbed are not allowed to experience any contact with liquid water prior to the analysis in the
805 lab. In other words, if the particles get in contact with liquid water after the adsorption step, the
806 adsorbed alkanes would desorb from the particles as they do it in the laboratory during melting.
807 Given the occurrence of wet/dry cycles in the source area (Ruth et al., 2007), we question the
808 plausibility of scenario A1. Moreover, we expect the characteristic desorption time to differ
809 between the three alkanes, which would be in contradiction to the observation that the alkane
810 ratios in the 1st and 2nd extraction are the same within the error limits.

811



812

813 *Figure 11: Diagrams of genetic fields for natural gas adopted from Milkov and Etiope (2018).* (a) Genetic
 814 diagram of $\delta^{13}\text{C-CH}_4$ versus $\text{CH}_4/(\text{C}_2\text{H}_6 + \text{C}_3\text{H}_8)$. Typical atmospheric values are indicated by a grey-shaded area,
 815 NGRIP values obtained from this study with a pink dot. (b) Methane genetic diagram of $\delta^{13}\text{C-CH}_4$ versus $\delta\text{D-CH}_4$.
 816 Values for cellulose (C), lignin (L) and pectin (P) from Vigano et al. (2009) and mean values for C3 and C4 plants,
 817 respectively, from studies by Keppler et al. (2006) and Vigano et al. (2009) are added.

818

819

820 (2) Microbial production

821 The second process that we take into consideration is the microbial production of excess alkanes
 822 through methanogenic microbes. Here we must again differentiate between two scenarios: a
 823 microbial production can either take place in the ice sheet itself (in situ) by extremophile
 824 microbes. This process requires that in situ produced excess alkanes are then adsorbed onto
 825 dust particles in the ice and subsequently slowly desorbed during extraction when in contact
 826 with liquid water (M1). Or the production takes place during the melt extraction when
 827 methanogenic microbes can metabolize in liquid water (*in extractu*; M2). Lee et al. (2020)
 828 already excluded a “simple” in situ production of excess CH_4 (microbial in situ production in
 829 the ice without an adsorption-desorption process; M0) and this option will therefore not be
 830 further discussed here.

831

832 The second part of a potential M1 process, the adsorption of the microbially produced excess
833 alkanes onto dust particles in the ice and the subsequent desorption during extraction, remains
834 difficult to assess. A selective adsorption of the in situ produced alkanes on mineral dust in the
835 ice requires that the in situ production is taking place on the dust particles themselves, which
836 can be questioned but cannot be ruled out. However, our ratios of excess
837 methane/ethane/propane in NGRIP and GRIP samples add another piece of corroborating
838 evidence that excess alkanes are not produced microbially. The main microbial production
839 process of methane, the decomposition of organic precursors in an anaerobic environment by
840 archaea, also co-produces ethane and propane, however only in marginal amounts. The typical
841 methanogenesis yields >200 times more methane than ethane and propane (Bernard et al., 1977;
842 Milkov and Etiope, 2018) while we find a molar ratio of methane to ethane to propane of 14:2:1
843 in our samples. This renders a microbial production pathway (in situ and *in extractu*, i.e. M1
844 and M2) unlikely. Moreover, a microbial production of CH₄ is unlikely in view of the $\delta^{13}\text{C}$ -
845 CH_{4(xs)} signature which is too heavy for microbial CH₄.

846 Similar to our argument made for the pure desorption hypothesis, the constant excess alkane
847 ratio in the second and first extraction is difficult to reconcile with an expected different
848 desorption lifetime for the three alkanes.

849
850 Apart from these quantitative limitations of microbial CH₄ in situ production in ice, there is
851 contradicting evidence from the “microbial inhibition experiment“ by Lee et al. (2020) also for
852 microbial production of alkanes during extraction. Lee et al. (2020) tested whether biological
853 CH_{4(xs)} production in the meltwater was inhibited when the ice core samples were treated with
854 HgCl₂. As CH_{4(xs)} was still observed in the poisoned samples and as it seems quite unlikely that
855 microbes are resistant to HgCl₂, this experiment questions the hypothesis of microbially
856 produced CH_{4(xs)} also during extraction (*in extractu*).

857
858 We conclude that regardless of the production pathway, in situ or *in extractu*, the fingerprint of
859 the produced excess alkanes in our samples (heavy $\delta^{13}\text{C}$ -CH_{4(xs)} signature and low
860 CH₄/(C₂H₆+C₃H₈) ratio) essentially rules out a microbial source and another (abiotic?) process
861 for excess alkane production is likely to exist.

862

863 **(3) Abiotic/ chemical production**

864 In this last section we consider an abiotic or chemical process to be responsible for the observed
865 excess alkanes, where excess alkanes would be produced through the abiotic decomposition of

866 labile organic compounds in the meltwater (C2). Based on the same arguments presented in the
867 previous section for a microbial in situ production, we also question an abiotic in situ production
868 in the ice (C1) as it would require the quantitative adsorption of the in situ produced alkanes
869 onto mineral dust particles but not the atmospheric CH₄ that is available in the ice otherwise.
870 However, as the location of an in situ excess CH₄ production in the ice is not the same as the
871 location of the bubble or clathrates in the ice, this argument is not able to exclude this
872 hypothesis. However, given the age of the ice that allows for permeation of gases on the grain
873 scale and the recrystallization of the ice during that time, which both could bring the
874 atmospheric CH₄ in contact with the dust particles, we feel this process is less plausible than a
875 potential C2 mechanism. Moreover (as mentioned before), in view of the expected different
876 desorption characteristics of the three alkanes we would expect different alkane ratios in the
877 1st and 2nd extraction, which is not the case. Accordingly, a direct abiotic production during the
878 melt process appears to be more likely than a desorption process.

879
880 Organic precursors for this abiotic production during extraction could be any organic matter
881 (either microbial or plant-derived). As the amount of excess alkanes is tightly coupled to the
882 amount of dust, we assume that these organic compounds are attached to dust particles. This
883 “docking” of the organic precursor onto the mineral dust could happen already in the dust
884 source region involving organic material available at the surface. Or it could happen by
885 adhering of volatile organic molecules or secondary organic aerosols from the atmosphere to
886 the mineral dust aerosol either before deflation at the source region or during transport to
887 Greenland.

888
889 We consider this pathway plausible, as in recent years the prevailing paradigm that methane is
890 only produced by methanogenic archaea under strictly anaerobic conditions has been
891 challenged. Several experimental studies demonstrated that methane can also be released from
892 dried soils (Hurkuck et al., 2012; Jugold et al., 2012; Wang et al., 2013; Gu et al., 2016), fresh
893 plant matter and dry leaf litter (Keppler et al., 2006; Vigano et al., 2008, 2009, 2010; Bruhn et
894 al., 2009; Derendorp et al., 2010, 2011), different kinds of living eukaryotes (plants, animals
895 and fungi) (Liu et al., 2015), single organic structural components (McLeod et al., 2008;
896 Messenger et al., 2009; Althoff et al., 2014) and in fact under aerobic conditions. Most of these
897 studies focused on methane, however, there is also evidence for simultaneous formation of other
898 short-chain hydrocarbons like ethane and propane (McLeod et al., 2008; Derendorp et al., 2010,
899 2011). At least three mechanisms have been identified to be relevant: i) photo-degradation, ii)

900 thermal degradation, or iii) degradation by the reaction with a reactive oxygen species (ROS)
901 (Schade et al., 1999; Wang et al., 2017). Common to all three pathways is a functional group
902 (for example a methyl or ethyl group) that is cleaved from the organic precursor molecule. Key
903 parameters that control the production of abiotic methane are mainly temperature, UV radiation,
904 water/ moisture, and the type of organic precursor material (Vigano et al., 2008; Derendorp et
905 al., 2010, 2011; Hurkuck et al., 2012; Jugold et al., 2012; Wang et al., 2013, 2017).

906

907 Recent findings demonstrated the large variety of potential organic precursors for abiotic trace
908 gas formation. For the formation of methane, the plant structural components pectin and lignin
909 have been identified in many studies as a precursor in different plant materials. Pectin and lignin
910 contain methoxyl-groups in two different chemical types, ester methoxyl (present in pectin) and
911 ether methoxyl (present in lignin) (Keppler et al., 2006, 2008; McLeod et al., 2008; Messenger
912 et al., 2009; Bruhn et al., 2009; Vigano et al., 2008; Hurkuck et al., 2012; Liu et al., 2015; Wang
913 et al., 2017). Ester methyl groups of pectin were also discovered as precursor for ethane
914 formation (McLeod et al., 2008). Overall, pectin makes up a large fraction of the primary cell
915 wall mass of many plants, thus, representing a large reservoir available as organic precursor for
916 abiotic alkane formation (Keppler et al., 2006; Mohnen et al., 2008; Vigano et al., 2008, 2010;
917 McLeod et al., 2008), and may be present in sufficient quantities in our ice core samples
918 attached to mineral dust particles. CH₄ production was also detected from cellulose even though
919 it does not contain methoxyl groups suggesting that other carbon moieties of polysaccharides
920 might allow abiotic CH₄ formation (Keppler et al., 2006; Vigano et al., 2008). In addition, poly-
921 unsaturated fatty acids in plant membranes are suggested to play a key role not only in the
922 formation of methane but also for ethane and propane (John and Curtis, 1977; Dumelin and
923 Tappel, 1977; Derendorp et al., 2010, 2011). Further, sulfur-bound methyl groups of
924 methionine are an important precursor for abiotic CH₄ formation in fungi (Althoff et al., 2014).

925

926 Considerably different emission rates were found for the same amount but different type of
927 organic substances leading to the conclusion that abiotic emissions are strongly dependent on
928 the type of organic precursor material or single structural components (Keppler et al., 2006;
929 McLeod et al., 2008; Vigano et al., 2008; Messenger et al., 2009; Hurkuck et al., 2012). Other
930 factors such as leaf and cell wall structure (McLeod and Newsham, 2007; Watanabe et al.,
931 2012; Liu et al., 2015) and the organic carbon content (Hurkuck et al., 2012) are suggested to
932 have an important influence on this process, too.

933

934 To explain the observed excess alkanes in dust-rich Greenland ice core samples by an abiotic
935 production through the decomposition of labile organic compounds requires adequate quantities
936 of organic precursors to be present within the ice core samples. Certainly, such material is
937 present in Greenland ice, but currently, there is no record on the amount and type of organic
938 substances in NGRIP and GRIP ice available. We have some limited information from
939 occasional Greenland ice core samples in which different types of organic substances were
940 detected (Giorio et al., 2018, and references therein), but it does not allow for an overarching
941 interpretation for our ice samples. A NGRIP record on formaldehyde and a GRIP record on
942 acetate and formate exists (Fuhrer et al., 1997), which suggest lower levels during the glacial,
943 but as we do not know which organic precursors lead to the excess CH₄ productions this
944 observation is only of limited value.

945
946 We may also question whether a perfect record of eligible precursor molecules could exist at
947 all. As we observe that precursor substances are labile and quickly decompose when in contact
948 with liquid water, a direct measurement of these substances might not be possible but only for
949 similar, non-reactive substances, which are then not qualified as precursors for the reaction
950 observed. The problems of sampling, analysis and interpretation of organic material in polar
951 ice are well summarized and expounded in Giorio et al. (2018).

952
953 In any case, it appears likely that the mineral dust carries along soil organic matter or plant
954 residues or accumulates organic aerosols as a result of organic aerosol aging during transport.
955 In our data we see a relationship between the amount of mineral dust within the ice core samples
956 and the amount of excess alkanes. As the amount of excess alkanes per Ca²⁺ (or mass of dust)
957 is variable, this suggests that mineral dust is just a carrier for (a variable amount of) organic
958 substances but does not account for the production of excess alkanes itself. The dust content
959 within the ice core sample can therefore only serve as a rough estimate of organic precursor
960 availability and whether an abiotic production from organic precursor substances is likely to
961 occur during extraction.

962
963 Again, our experiments can shed some light on the viability of this pathway for excess alkane
964 production. If we assume that the dust-related organic matter in the ice represents a reservoir
965 available for an abiotic production, then the decomposition continues until all functional groups
966 are cleaved from their organic precursor molecules and released as excess alkanes. Once the
967 reservoir is emptied excess alkane production ceases (Derendorp et al., 2010, 2011). In line, we

968 interpret that the decrease in the amount of measured excess alkanes from the 1st to the 2nd
969 extraction may result from an exhaustion of the precursor reservoir. The reaction time is slow
970 enough to allow for the continuing production during the second extraction but too slow for a
971 detectable production during continuous flow analysis of CH₄, where the water phase is present
972 only for less than two minutes before gas extraction. The significantly reduced production
973 during the 2nd extraction in our samples shows that the time scale for this process is hours (see
974 Fig. C1) until the reservoir of functional groups is depleted. We note that this implies that the
975 amount of excess alkanes is strongly dependent on the time span when liquid water is in contact
976 with the dust, which varies among the methods used for CH₄ analyses. Thus, any excess CH₄
977 in measurements from different labs performed under different conditions may differ.

978

979 To explain an abiotic alkane production, certain conducive boundary conditions must be met.
980 The most important parameters that control non-microbial trace gas formation are temperature
981 and UV radiation. This was demonstrated in many field and laboratory experiments (Keppler
982 et al., 2006; McLeod et al., 2008; Vigano et al., 2008, 2009; Messenger et al., 2009; Bruhn et
983 al., 2009; Derendorp et al., 2010, 2011; Hurkuck et al., 2012; Jugold et al., 2012; Wang et al.,
984 2017). Generally, increasing temperatures lead to exponentially increasing CH₄ emissions
985 (Vigano et al., 2008; Bruhn et al., 2009; Wang et al., 2013; Liu et al., 2015). The same behaviour
986 was observed for ethane and propane with very low emissions at ambient temperatures (20-
987 30°C) and a maximum at 70°C (McLeod et al., 2008; Derendorp et al., 2010, 2011). At constant
988 temperatures emission rates decreased over time, which is at high temperatures on the timescale
989 of hours and at ambient temperatures of months. Even after months, some production was
990 observed, pointing to a slowly depleting reservoir of organic precursors (Derendorp et al., 2010,
991 2011). Increasing emissions observed at temperatures >40°C were also used as indicator to
992 exclude the possibility of enzymatic activity, as the denaturation of enzymes would lead to
993 rapidly declining emissions at higher temperatures (Keppler et al., 2006; Derendorp et al., 2011;
994 Liu et al., 2015). We note that our sample extraction takes place at 0°C or a few °C above,
995 hence, temperature conditions during the extraction are not conducive of the type of abiotic
996 alkane production as observed in the studies listed above. Whether the cool temperature of the
997 meltwater during extraction inhibits abiotic reaction is difficult to say. Derendorp et al. (2010,
998 2011) observed a much lower temperature dependency of C₂-C₅ hydrocarbon emissions from
999 ground leaves than whole leaves, which might also apply to our samples with very fine
1000 fragments of organic substances attached to dust particles.

1001

1002 Besides the strong relationship to temperature also UV irradiation seems to have a substantial
1003 effect on an abiotic production. Studies on irradiated samples (dry and fresh plant matter, plant
1004 structural components) showed a linear increase in methane emissions, while UV-B irradiation
1005 seems to have a much stronger effect on the release compared to UV-A (Vigano et al., 2008;
1006 McLeod et al., 2008; Bruhn et al., 2009; Jugold et al., 2012). The influence of visible light (400-
1007 700 nm), however, seems controversial (Keppler et al., 2006; Bruhn et al., 2009; Austin et al.,
1008 2016). Further, samples that were heated and irradiated show a different emission curve than
1009 just heated samples, indicating that irradiation changes the temperature dependency, in turn
1010 pointing to the fact that different chemical pathways exist (Vigano et al., 2008).

1011 In dark experiments on plant material at different temperatures CH₄ emissions were still
1012 observed, while again higher temperatures revealed much higher emissions, emphasizing the
1013 strong temperature dependency also without UV irradiation (Vigano et al., 2008; Wang et al.,
1014 2008; Bruhn et al., 2009). The release of ethane along with methane from pectin was also
1015 stimulated under UV radiation (McLeod et al., 2008).

1016

1017 Regarding our measurements, the sample vessel in the $\delta^{13}\text{C}$ -CH₄ device is encased by a UV
1018 blocker foil absorbing the shortwave (<600 nm) emissions from the heating bulbs when melting
1019 the ice sample, while in the δD -CH₄ device the sample vessel is completely shielded from light
1020 (Sect. 2.2 and 2.3). Two NGRIP ice core samples were measured with the $\delta^{13}\text{C}$ -CH₄ device in
1021 the dark (“dark extraction”) showing the same amount of excess alkanes as the regular
1022 measurements at day light. This indicates that light >600 nm has no influence on an *in extractu*
1023 reaction during our measurements.

1024

1025 We stress that although we can exclude a direct UV effect during sample extraction, it is
1026 possible that UV irradiation during dust aerosol transport to Greenland and within the upper
1027 snow layer after deposition until the snow gets buried into deeper layers may precondition
1028 organic precursors attached to mineral dust to allow for alkane production to occur during
1029 extraction. In particular, the first step of the reaction (excitation of the homolytic bond of a
1030 precursor compound) may start already in the atmosphere or in the upper firn layer where
1031 energy from UV radiation is available. Within the ice sheet the reaction may be paused (“frozen
1032 reaction”) and the total reaction pathway is only completed during the melting process when
1033 liquid water is present.

1034

1035 Finally, we consider the role of reactive oxygen species in an abiotic production pathway. ROS
1036 are widely produced in metabolic pathways during biological activity but also during

1037 photochemical reactions with mineral oxides (Apel and Hirt, 2004; Messenger et al., 2009;
1038 Georgiou et al., 2015). Through their high oxidative potential ROS are capable to cleave
1039 functional groups from precursor compounds. Several studies have demonstrated this
1040 mechanism for the production of abiotic CH₄ in soils and plant matter (McLeod et al., 2008;
1041 Messenger et al., 2009; Althoff et al., 2010, 2014; Jugold et al., 2012; Wang et al., 2011, 2013)
1042 and for other trace gases such as CO₂, ethane, and ethylene from plant pectins (McLeod et al.,
1043 2008). UV radiation or thermal energy has no direct influence on the degradation process by
1044 the reaction with ROS, however, it might also be a stimulating factor and evoke further indirect
1045 reactions. For instance, UV radiation can lead to changes in plants which in turn lead to ROS
1046 generation (Liu et al., 2015). It was demonstrated that UV radiation induces the formation of
1047 organic photosensitizers or photo-catalysts which increase CH₄ emissions from pectin
1048 (Messenger et al., 2009) and clay minerals. For example, the formation of OH from
1049 montmorillonite and other clay minerals upon UV (and visible light) irradiation shows that
1050 clays might play a significant role in the oxidation of organic compounds on their surface in
1051 different environments (Katagi, 1990; Wu et al., 2008; Kibanova et al., 2011).

1052

1053 It has been proven that the species type and the overall amount of ROS available for, or involved
1054 in a reaction, has a significant effect on the amount of emissions through such a process (Jugold
1055 et al., 2012; Wang et al., 2013, 2017). For the production of methane (and ethane), hydrogen
1056 peroxide (H₂O₂) and hydroxyl radicals (OH) have been proven to be the prominent species
1057 (Messenger et al., 2009; Althoff et al., 2010; Wang et al., 2011, 2013; Jugold et al., 2012;
1058 McLeod et al., 2008). Such ROS could be already present in the snow and ice or being produced
1059 in the meltwater. For example, H₂O₂ can be unambiguously detected in Greenland Holocene
1060 ice using CFA, however, H₂O₂ in dusty glacial ice is mostly below the detection limit, likely
1061 due to oxidation reactions in the ice sheet or during melt extraction.

1062

1063 In summary, we believe that in our case of excess alkane production/ release in the meltwater
1064 at low temperatures and without any UV irradiation, the ROS-induced mechanism appears
1065 possible. In experiments with plant pectin McLeod et al. (2008) observed not only CH₄ but also
1066 ethane and found a methane to ethane production ratio of around 5 which is similar to our value
1067 of around 7. Accordingly, we see that a ROS-induced production pathway has the potential to
1068 explain excess alkanes in our samples, however, little is known about ROS chemistry in ice
1069 cores in particular for reactions with organic precursors and more research is needed to
1070 understand the role of ROS in organic decomposition in ice. Another alternative to the two-

1071 stage reaction pathway with ROS would be a reaction catalyzed in the meltwater by dust-
1072 derived transition metals. This has been observed for example for the oxidation of SO₂ in water-
1073 activated aerosol particles (Harris et al., 2013), but to our knowledge it has not been described
1074 in the literature for alkane production via organic precursors so far. Accordingly, we can only
1075 speculate on this pathway at the moment.

1076

1077

1078 Another key parameter influencing all abiotic pathways might be the presence of liquid water
1079 or moisture. In experiments testing the hypothesis of non-microbial CH₄ formation in different
1080 soil samples, it was demonstrated that the addition of water/moisture led to an up to eight-fold
1081 increase in CH₄ emissions (Hurkuck et al., 2012; Jugold et al., 2012; Wang et al., 2013). It is
1082 hypothesized that the presence of liquid water or moisture stimulates (in addition to heating or
1083 UV radiation) the cleaving process of a functional group from the primary precursor compound
1084 and therefore increases the production of CH₄. However, it seems that the stimulating effect by
1085 water cannot be generalized, as Wang et al. (2013) emphasized that this process is highly
1086 dependent on “water of proper amount”. In their experiments, CH₄ emissions from peat and
1087 grassland soil samples treated with a varying amount of water in oxic–anoxic cycles at 70°C
1088 were measured. They observed that under both aerobic and anaerobic conditions water does not
1089 always stimulate non-microbial CH₄ release and that too much water can also suppress CH₄
1090 emissions. Wang et al. (2013) observed differences between different soil samples in response
1091 to a varying water content indicating that the water effect is different for different precursors.
1092 With respect to our observations on NGRIP and GRIP samples the presence of water seems to
1093 be a fundamental parameter influencing the second step of a “frozen reaction” *in extractu*
1094 process, where the duration of water presence plays an important role.

1095

1096 A final puzzle piece for a possible abiotic methane production comes from our dual isotopic
1097 fingerprints of the excess CH₄. As illustrated in Fig. 11 (right panel) our $\delta\text{D-CH}_{4(\text{xs})}$ signature
1098 lies well within the distribution of the hydrogen isotopic composition of CH₄ produced from
1099 potential organic precursors. For $\delta^{13}\text{C}$ our values lie outside and on the heavier side of the
1100 isotopic carbon signature spectrum.

1101

1102 We conclude that despite our inability to pinpoint the exact organic precursors that lead to
1103 abiotic excess alkane production during the melt extraction of our ice samples at this point, both
1104 the ratio of the excess alkanes as well as the isotopic signature of excess CH₄ is generally in

1105 line with this pathway. Thus, without further contradicting evidence from targeted studies on
 1106 organic precursors in ice core samples and their chemical degradation, we believe that the ROS-
 1107 induced production pathway is to date the most likely explanation for the observed excess
 1108 alkanes during extraction. However, we cannot completely rule out an adsorption-desorption
 1109 process of thermogenic gas on dust particles.

1110
 1111
 1112
 1113
 1114
 1115
 1116
 1117

Table 1: **Overview of the different hypotheses explaining the possible sources for excess alkanes (as illustrated in Figure 10) in relation to our experimental and analytical observations.** A green checkmark indicates that the observation is in line with the respective mechanism, a black cross indicates that the observation is in not line with the respective mechanism. A grey shaded area means that this observation does not apply or does not affect the respective mechanism.

	(1) ADSORPTION- DESORPTION OF THERMOGENIC/ ATMOSPHERIC GAS		(2) MICROBIAL PRODUCTION			(3) ABIOTIC/ CHEMICAL PRODUCTION	
	A1	A2	M0	M1	M2	C1	C2
Correlation to Ca ²⁺ / mineral dust	✓	✓	✓	✓	✓	✓	✓
Alkane pattern	✓	✗	✗	✗	✗	(✓)	(✓)
CFA evidence			✗				
$\delta^{13}\text{C-CH}_{4(x\text{s})}$	✗	✓	✗	✗	✗	(✓)	(✓)
$\delta\text{D-CH}_{4(x\text{s})}$	✓	✗	✓	✓	✓	(✓)	(✓)
$\delta\text{D-CH}_{4(x\text{s})}$ estimated by Lee et al. (2020)	✓	✗	✓	✓	✓	(✓)	(✓)
Poisoning experiment by Lee et al. (2020)					✗		

1118
 1119
 1120
 1121

5. Conclusions and Outlook

1122 The comparison of methane records from ice cores samples measured with different extraction
 1123 techniques requires careful consideration and interpretation. Non-atmospheric methane
 1124 contributions to the total methane concentration were discovered in specific Greenland ice core
 1125 sections pointing to a process occurring during the wet extraction. To better assess this finding,
 1126 we measured new records of [methane], [ethane], [propane], $\delta\text{D-CH}_4$, and $\delta^{13}\text{C-CH}_4$ on discrete
 1127 NGRIP and GRIP ice core samples using two different wet extraction systems. With our new

1128 data we confirm the production of CH_{4(xs)} in the meltwater and quantify its dual isotopic
1129 signature. With the simultaneous detection of ethane and propane we discovered that these
1130 short-chain alkanes are co-produced in a fixed molar ratio pointing to a common production
1131 pathway. With our 2nd extraction we constrained the temporal dynamics of this process, which
1132 occurs on the timescale of hours.

1133

1134 Based on our new experimental data we provide an improved assessment of several potential
1135 mechanisms that could be relevant for the observed variations in NGRIP and GRIP ice samples.
1136 A microbial CH₄ production represents in principle an obvious candidate but regardless of
1137 whether this CH₄ is produced in situ or *in extractu*, several lines of evidence gained from our
1138 measurements (low CH₄/(C₂H₆+C₃H₈) ratio, heavy δ¹³C-CH_{4(xs)} signature) demonstrate that the
1139 fingerprint of the produced excess alkanes is unlikely to have a microbial source. Also an
1140 adsorption-desorption process of atmospheric or thermogenic CH₄ on dust particles does not
1141 match many of our observations and is therefore unlikely. However, with the current knowledge
1142 we cannot definitely exclude such an adsorption of thermogenic gas to be responsible for the
1143 observed excess alkane levels in our samples.

1144

1145 At present we favor to explain the formation of excess alkanes by abiotic decomposition of
1146 organic precursors during prolonged wet extraction. Such an abiotic source for methane and
1147 other short-chain alkanes was discovered previously in other studies (Keppler et al., 2006;
1148 Vigano et al., 2008, 2009, 2010; Messenger et al., 2009; Hurkuck et al., 2012; Wang et al.,
1149 2013, and others listed above) using different organic samples, e.g. from plant or soil material,
1150 however, this process has not been connected to excess CH₄ production during ice core
1151 analyses. This process matches many of our observations and such a mechanism can be
1152 responsible for excess alkanes in Greenland ice core samples. To better assess a potential abiotic
1153 production process in ice analyses the most important questions to solve in the future are: What
1154 are the specific precursor substances? Which parameters control an abiotic production during
1155 wet extractions? How does the fixed molar ratio between methane, ethane, and propane come
1156 about in this process? And finally, in which way is this excess alkane production causally
1157 related to the amount of mineral dust within the ice sample?

1158

1159 Identifying a specific reaction pathway that leads to the short-chain alkanes with their observed
1160 ratios would certainly benefit from identifying targeted organic precursor substances in the ice.
1161 However, detecting these postulated organic precursors in the ice core is inherently difficult as

1162 these compounds must be very labile in water as our experiments demonstrated that after about
1163 30 min only a fraction of these compounds remains in the meltwater while the majority already
1164 reacted to excess alkanes. Future studies may also focus on further isotopic measurements
1165 ($\delta^{13}\text{C-CH}_4$ and $\delta\text{D-CH}_4$) including isotope labeling experiments providing an option to
1166 unambiguously detect methane produced during the measurement procedure in a commonly
1167 used wet extraction technique, and again, to uncover potential reaction mechanisms for $\text{CH}_{4(\text{xs})}$
1168 production.

1169

1170 To better assess the viability of the alternative hypothesis of a release of previously adsorbed
1171 alkanes from dust particles (scenario A1 and A2) during the extraction, dust particles from the
1172 Taklamakan or Gobi desert need to be tested whether they contain relevant amounts of adsorbed
1173 alkanes that are released when in contact with liquid water. A second step could be to expose
1174 such dust samples to high levels of alkanes to mimic the adsorption process of natural gas seeps.
1175 It also needs to be shown that the adsorbed alkanes stay adsorbed on the dust particles for a
1176 prolonged time (months, ideally years) after exposing the particles to ambient air and that
1177 droplet and ice nucleation during aerosol transport does not lead to a loss of the previously
1178 adsorbed CH_4 . To quantify any isotopic fractionation involved with the ad- and desorption step,
1179 $\delta^{13}\text{C-CH}_4$ and $\delta\text{D-CH}_4$ analyses will be most valuable.

1180

1181 Finally, our studies clearly show that the published Greenland ice core CH_4 record is biased
1182 high for selected (glacial, dust-rich) time intervals and needs to be corrected for the excess CH_4
1183 contribution. This is particularly important for studies of the IPD in CH_4 and stable isotope
1184 ratios of methane. Methodological ways to remedy excess methane (and ethane and propane)
1185 in future measurements of atmospheric $[\text{CH}_4]$ from air trapped in ice cores could be to use
1186 continuous online CH_4 measurements, which apparently avoid sizeable $\text{CH}_{4(\text{xs})}$ production. But
1187 also dry extraction methods and sublimation techniques for discrete samples, which are
1188 expected to avoid *in extractu* production by evading the melting phase, could be used. Finally,
1189 our own $\delta^{13}\text{C-CH}_4$ device, which allows to measure $\delta^{13}\text{C-CH}_4$ as well as methane, ethane, and
1190 propane concentrations from the same sample, can be used to correct the measured CH_4 values
1191 making use of the co-production of the other two alkanes.

1192

1193 It is clear that $\text{CH}_{4(\text{xs})}$ needs to be corrected for when interpreting the already existing discrete
1194 CH_4 records and its stable isotopes in dust-rich intervals in Greenland ice core samples. Impact
1195 of $\text{CH}_{4(\text{xs})}$ on interpreting past atmospheric $[\text{CH}_4]$ will only slightly affect radiative forcing

1196 reconstructions, however, it will have a significant effect on the assessment of the global CH₄
1197 cycle and in particular on the hemispheric CH₄ source distribution which is based on the IPD.
1198 We observe that in some intervals CH_{4(xs)} is in the same range as the previously reconstructed
1199 IPD implying that correcting for CH_{4(xs)} will lower the IPD considerably and hence lower also
1200 the relative contribution of northern hemispheric sources at those times. We see that there is the
1201 urgent need to reliably revisit Greenland ice core CH₄ records for the excess CH₄ contribution
1202 and in future work we aim to establish an applicable correction for excess methane (CH_{4(xs)},
1203 $\delta^{13}\text{C-CH}_4(\text{xs})$, $\delta\text{D-CH}_4(\text{xs})$) in existing records using the co-production ratios of methane, ethane,
1204 and propane, the isotopic mass balance of excess and atmospheric CH₄ in ice core samples as
1205 well as the overall correlation of excess CH₄ with the mineral dust content in the ice.

1206

1207

1208

1209

1210

1211

1212

1213

1214

1215

1216

1217

1218

1219

1220

1221

1222

1223

1224

1225

1226

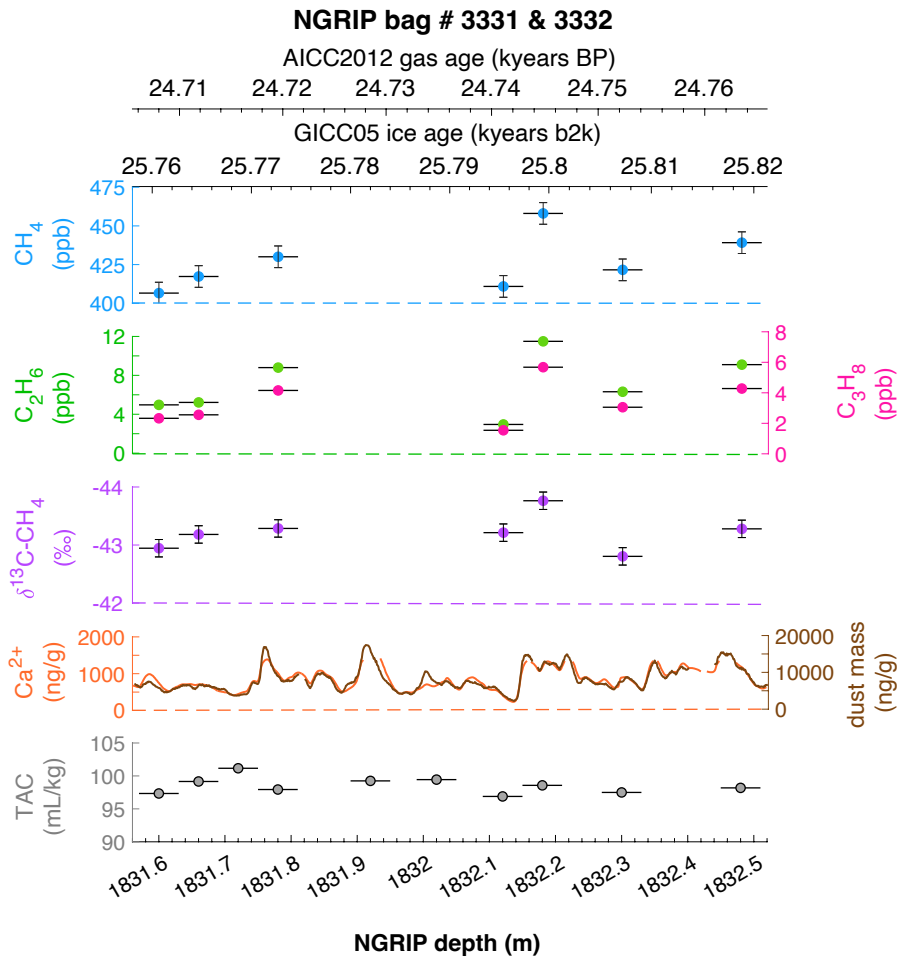
1227

1228

1229

1230 **Appendix A**

1231

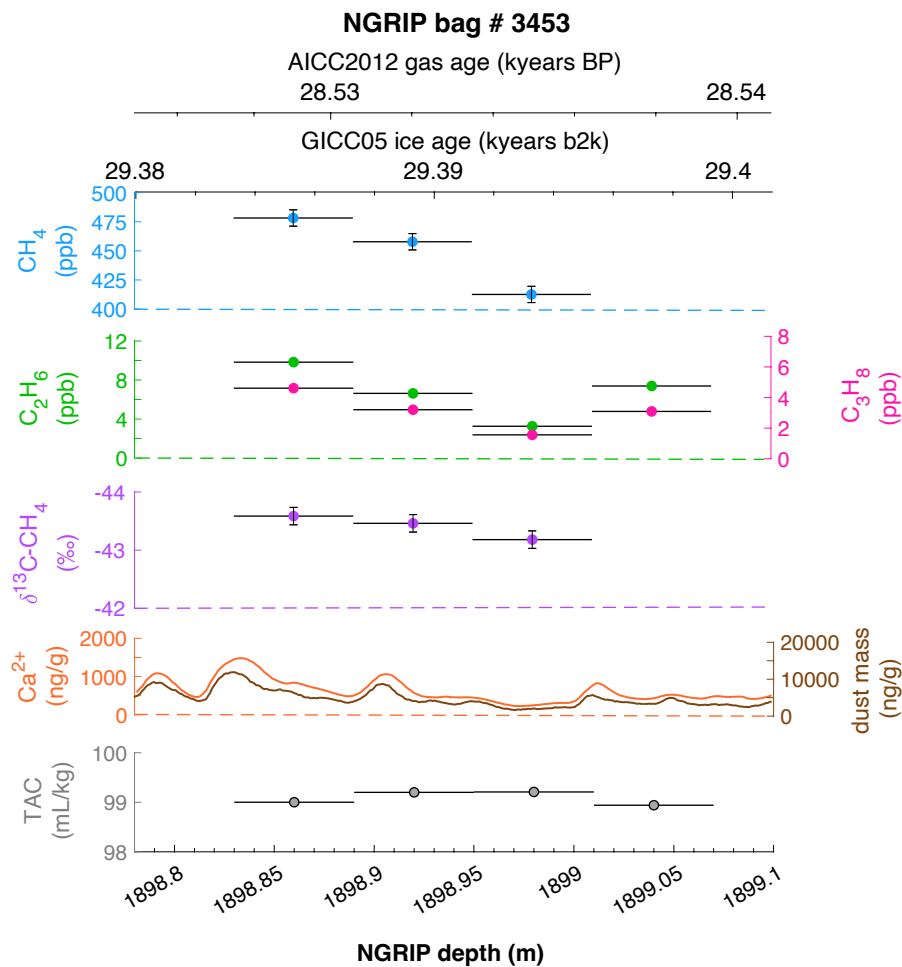


1232

1233 Figure A1: **Detailed data overview for the neighbouring NGRIP bags 3331 & 3332.** Bag-specific overview of
1234 several parameters measured for each sample in this bag: methane, ethane, propane, Ca²⁺, mineral dust mass, TAC
1235 (Total Air Content), $\delta^{13}\text{C-CH}_4$, indicated at the NGRIP depth (bottom axis) and the AICC2012 gas age (upper top
1236 axis) and the GICC05 ice age (lower top axis). The mineral dust record is taken from Ruth et al. (2003), the Ca²⁺
1237 record from Erhardt et al. (2022).

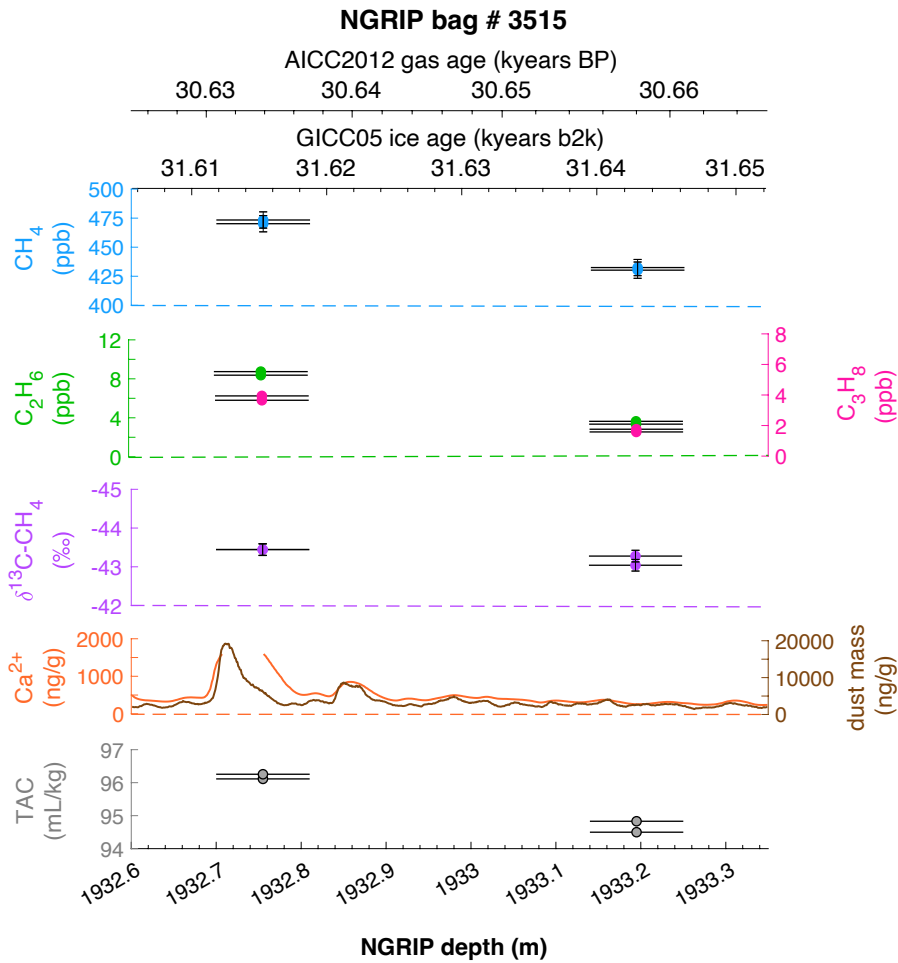
1238

1239



1240
1241
1242
1243
1244
1245
1246
1247
1248
1249

Figure A2: **Detailed data overview for NGRIP bag 3453.** Bag-specific overview of parameters measured for each sample in this bag: methane, ethane, propane, Ca^{2+} , mineral dust mass, TAC (Total Air Content), $\delta^{13}\text{C-CH}_4$, indicated at the NGRIP depth (bottom axis) and the AICC2012 gas age (upper top axis) and the GICC05 ice age (lower top axis). The mineral dust record is taken from Ruth et al. (2003), the Ca^{2+} record from Erhardt et al. (2022).

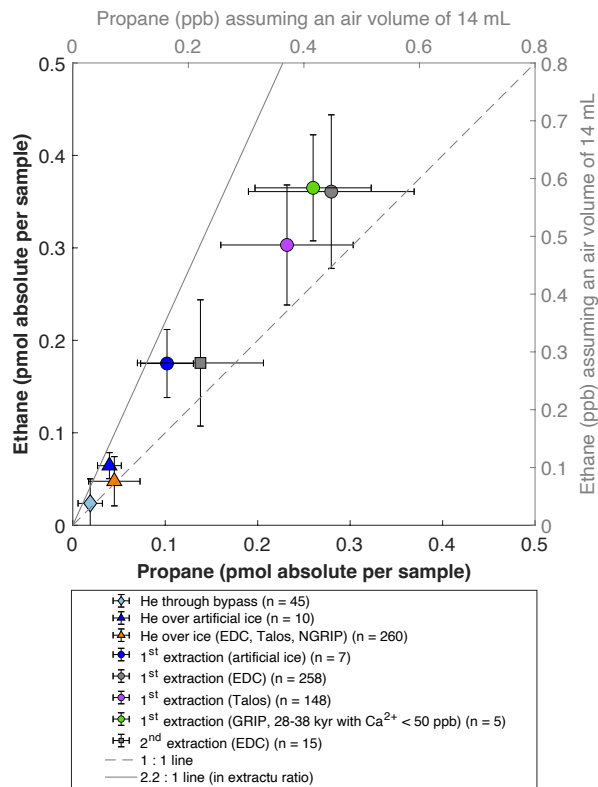


1250
 1251
 1252
 1253
 1254
 1255
 1256
 1257
 1258
 1259
 1260
 1261
 1262
 1263
 1264
 1265
 1266
 1267
 1268
 1269
 1270
 1271

Figure A3: **Detailed data overview for NGRIP bag 3515.** Bag-specific overview of parameters measured for each sample in this bag: methane, ethane, propane, Ca^{2+} , mineral dust mass, TAC (Total Air Content), $\delta^{13}\text{C-CH}_4$, indicated at the NGRIP depth (bottom axis) and the AICC2012 gas age (upper top axis) and the GICC05 ice age (lower top axis). The mineral dust record is taken from Ruth et al. (2003), the Ca^{2+} record from Erhardt et al. (2022). Note that there is a gap in the Ca^{2+} record which was corrected by a fill routine for the analysis of the two measured samples at this depth.

1272 **Appendix B**

1273



1274

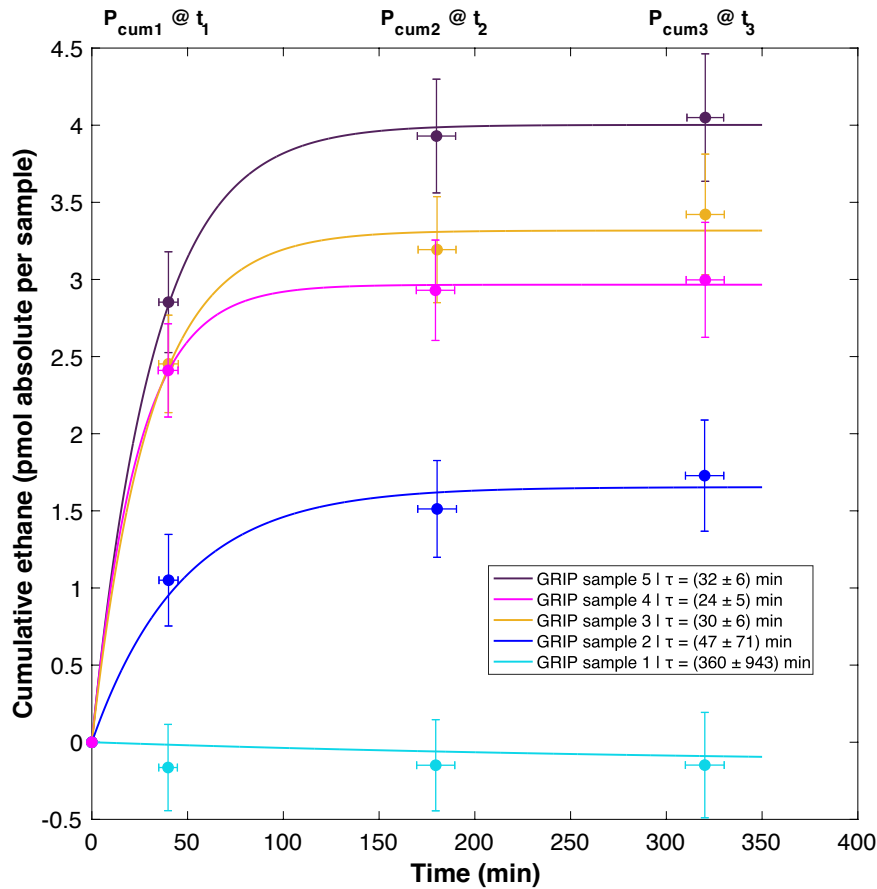
1275 **Figure B1: Collection of different measurement modes and ice core sample locations to estimate individual**
 1276 **blank contributions.** The mode “He through bypass” (diamond) refers to a measurement type where helium is
 1277 injected into our system but without flowing through our extraction vessel. “He over ice” (triangles) refers to
 1278 helium injections over the unmelted ice core sample. Results from the 1st extraction are shown for different ice
 1279 cores (artificial gas-free ice, Talos Dome, EDC, GRIP; colored circles). The 2nd extraction of the Antarctic EDC
 1280 ice core is marked as grey square. Lines with ethane/propane ratios are for orientation only.

1281

1282 In this section we provide background information of how we determined the blank
 1283 contributions for our alkane measurements for the different measurement modes. Overall, our
 1284 strategy is similar to the measurements which were published earlier in 2014 (Schmitt et al.,
 1285 2014). Here we include more measurements performed since then with our $\delta^{13}\text{C}\text{-CH}_4$ device.
 1286 Following the classic usage, blank contributions are related to the measurement device itself
 1287 rather than to the sample, thus we report the measured values of the species as absolute amount
 1288 in pmol with respect to a measurement procedure (sample run). To compare these absolute
 1289 values with the classic units of species concentration in the air for an ice sample in ppb, Fig.
 1290 B1 has secondary axes (grey) for the species concentrations in ppb for an assumed sample size
 1291 of air of 14 mL STP (our typical ice core sample size).

1292 Since our extraction device is at vacuum conditions, a blank contribution from leaks that allow
 1293 ambient air with relatively high ethane and propane concentrations to be collected together with
 1294 our sample seems the most straightforward risk. To quantify this leak contribution, we routinely

1295 perform so called “He over ice” runs where a helium flow is passed over the unmelted ice core
1296 sample and the species are trapped on the cold activated carbon trap (see details in Schmitt et
1297 al., 2014). The trapping duration is the same as for the 1st extraction, thus this “He over ice”
1298 run mimics the contribution for the 1st extraction. As can be seen in Fig. B1, for ethane this
1299 “leak contribution” is typically <0.1 ppb, thus small compared to concentrations we see for
1300 dust-rich Greenland ice samples with about 6 ppb (see Fig. 5). However, this “He over ice”
1301 does not capture the actual melting process of the ice sample and represents the lowest blank
1302 boundary for our ice core samples. To mimic the full procedure an ice core samples experiences,
1303 we run a limited number of artificial gas-free ice samples (blue circles in Fig. B1). The ethane
1304 values obtained for these artificial ice sample is around 0.3 ppb and thus considerably higher
1305 than for the procedure without melting. This indicates that the presence of liquid water may
1306 lead to a desorption or production of alkanes from the inner walls of our extraction vessel.
1307 Alternatively, our artificial ice still contains traces of alkanes. So far, we could not solve this
1308 issue and more experiments are needed. A much larger data set on the upper boundary of the
1309 extraction blank comes from routine measurements of Antarctic ice core samples with the
1310 primary target of stable isotope analyses of CH₄ and N₂O. These Antarctic samples cover glacial
1311 and interglacial time intervals and the measured ethane values are typically around 0.55 ppb.
1312 Since the reconstructed atmospheric background for ethane in Antarctic ice is lower with values
1313 in the range of 0.1 – 0.15 ppb for the late Holocene (Nicewonger et al., 2018), a realistic blank
1314 contribution for our 1st extraction is on the order of 0.4 to 0.5 ppb. An additional constraint
1315 comes from five stadial GRIP samples from the time interval 28-38 kyears (green circle in Fig.
1316 B1) that have very low Ca²⁺ content (< 50 ppb) and thus have likely a negligible contribution
1317 from a dust-related *in extractu* component. The measured ethane concentration from these
1318 GRIP samples is very similar to the Antarctic ice core samples. One possible explanation would
1319 be that the atmospheric ethane concentration during the glacial was similar and low for both
1320 hemispheres. Regardless of the individual contributions, for our considerations of dust-related
1321 *in extractu* production in Greenland ice cores the upper estimate for the sum of atmospheric
1322 background and blank contribution is about 0.55 ppb (about 0.35 pmol) for ethane. Since the
1323 ethane to propane ratio for these non-dust contributions is about 1.5, the corresponding propane
1324 values are lower by that value. Importantly, since the ethane to propane ratio for our dust-related
1325 production is with 2.2 rather similar, its impact on the calculated ethane to propane ratio (e.g.
1326 Fig. 4) is very minor and small within the error estimate. For that reason, we did not correct our
1327 Greenland measurements for any blank contribution and showed the values as measured along
1328 with measurements of Antarctic ice cores samples which serve as first-order blank estimates.



1331

1332

1333 Figure C1: **Temporal dynamics of excess ethane production in GRIP ice core samples.** Cumulative ethane
 1334 amount from the 1st, 2nd, and 3rd extraction in relation to the time available for a potential reaction in the meltwater
 1335 during each extraction. We assume a first-order reaction kinetic as model for our observations where the mean
 1336 half-life time (τ) and standard deviations are calculated for each GRIP sample from the compilation of all 1000
 1337 iterations of our Monte Carlo approach. The numbered samples can also be found in Fig. 7a.
 1338

1339 The general equation to describe a first-order chemical reaction or exponential decay process
 1340 (e.g. release of adsorbed gas from the adsorbent) is Eqn. (1).

1341

$$1342 \quad N(t) = N_0 * e^{(-t/\tau)} \quad (1)$$

1343

1344 With N_0 being the total amount of substance (reactant) at the start of the reaction. $N(t)$ equals
 1345 the remaining amount of the reactant at time t , and t being time of reaction and τ , the mean
 1346 lifetime of the reaction. In our case, we cannot determine $N(t)$ neither do we know N_0 but we
 1347 experimentally determined the cumulative amount of the product, $P_{cum(t)}$, at three different times
 1348 as our observable quantity. Thus, in Eqn. 2 we define $P_{cum(t)}$ as the difference between N_0 and
 1349 $N(t)$.

1350

1351
$$P_{\text{cum}(t)} = N_0 - N(t) \quad (2)$$

1352

1353 Replacing $N(t)$ in Eqn. 1 with our definition in Eqn. 2 we obtain Eqn. 3, which contains two fit
1354 parameters, N_0 and τ , as well as our observable parameter $P_{\text{cum}(t)}$, i.e. the cumulative amount of
1355 alkane for a certain time step.

1356

1357
$$P_{\text{cum}(t)} = N_0 - N_0 * e^{-t/\tau} \quad (3)$$

1358

1359 For the five GRIP samples we have three consecutive measurements each, the 1st, 2nd, and 3rd
1360 extraction. The time dependent $P_{\text{cum}(t)}$ values are as follows: $P_{\text{cum}0}$ is defined as 0, representing
1361 the state of the unmelted ice sample before liquid water is present. $P_{\text{cum}1}$ is the measured amount
1362 from the 1st extraction (ice extraction) minus the estimated contribution from the atmosphere
1363 and minus the blank contribution for the 1st extraction. $P_{\text{cum}2}$ is the sum of $P_{\text{cum}1}$ and the value
1364 from the 2nd extraction minus the blank contribution of the 2nd extraction. Similarly, $P_{\text{cum}3}$ is the
1365 sum of $P_{\text{cum}2}$ and the value from the 3rd extraction minus the blank for the 3rd extraction.

1366 To account for the uncertainties of the involved measurements and corrections, we added
1367 normally distributed errors to the following parameters (measured value $\pm 5\%$; blank $\pm 20\%$;
1368 atmospheric contribution $\pm 50\%$), and we also assigned an uncertainty of 5 min to the time to
1369 account for variations of the melting speed of the ice and delays between the individual
1370 measurements (1st, 2nd, 3rd).

1371 For the fitting procedure we used the Matlab built in nonlinear least-squares solver called
1372 'lsqcurvefit' and performed 1000 runs where we varied the above-mentioned input parameters.
1373 The output of the function are the two fit parameters, i.e., N_0 and τ . From the 1000 runs we
1374 calculated the mean and the 1 sigma standard deviation of the lifetime.

1375

1376 Note, this approach can only be suitably applied to ethane and propane as the past atmospheric
1377 contribution for these gases in the 1st extraction is typically small against the excess contribution
1378 for dust-rich samples. For our five GRIP samples, where we have three consecutive extractions,
1379 four samples are considered "dust-rich" and are suitable to provide robust estimates for τ . In
1380 contrast, one sample is from an interstadial period with very low dust content and thus shows
1381 negligible production of alkanes in all three extractions. While this sample is not suited to
1382 provide robust estimates for τ , this sample allows to assess the first-order plausibility of the
1383 blank correction and the assumed atmospheric background for ethane for the 1st extraction

1384 (sample number 1, bottom-most sample). For a sample without any *in extractu* production, the
1385 cumulative curve should be flat at around 0 which is the case within our error estimates.

1386

1387

1388

1389

1390

1391

1392

1393

1394

1395

1396

1397

1398

1399

1400

1401

1402

1403

1404

1405

1406

1407

1408

1409

1410

1411

1412

1413

1414

1415

1416

1417

1418 **Code availability**

1419 No special code related to the manuscript.

1420

1421 **Data availability**

1422 Data is provided on request to the authors.

1423

1424 **Author contribution**

1425 The experimental approach was defined by JS, HF and MM. MM and BS performed the
1426 measurements; MM and JS analyzed the data; MM wrote the manuscript draft; MM prepared
1427 the manuscript with contributions from all co-authors.

1428

1429 **Competing interests**

1430 The authors declare that they have no conflict of interest.

1431

1432 **Disclaimer**

1433 None.

1434

1435 **Special issue statement**

1436 Ice core science at the three poles (CP/TC inter-journal SI)

1437

1438 **Acknowledgments**

1439 We thank Murat Aydin for very helpful review comments. The research leading to these results
1440 has received funding from the Swiss National Science Foundation (no. 200020_172506 &
1441 200020B_200328). This work is a contribution to the NorthGRIP ice core project, which is
1442 directed and organized by the Department of Geophysics at the Niels Bohr Institute for
1443 Astronomy, Physics and Geophysics, University of Copenhagen. It is supported by funding
1444 agencies in Denmark (SNF), Belgium (FNRS-CFB), France (IFRTP and NSU/CNRS),
1445 Germany (AWI), Iceland (RannIs), Japan (MEXT), Sweden (SPRS), Switzerland (SNF), and
1446 the United States (NSF).

1447

1448 **References**

1449

1450 Althoff, F., Jugold, A. and Keppler, F.: Methane formation by oxidation of ascorbic acid
1451 using iron minerals and hydrogen peroxide. *Chemosphere* 80, 286–292,
1452 <https://doi.org/10.1016/j.chemosphere.2010.04.004>, 2010

1453

1454 Althoff, F., Benzing, K., Comba, P., McRoberts, C., Boyd, D. R., Greiner, S. and Keppler, F.:
1455 Abiotic methanogenesis from organosulphur compounds under ambient conditions, *Nat*
1456 *Commun*, 5, 4205, <https://doi.org/10.1038/ncomms5205>, 2014
1457

1458 Anklin, M., Barnola, J.-M., Schwander, J., Stauffer, B., and Raynaud, D.: Processes affecting
1459 the CO₂ concentrations measured in Greenland ice, *Tellus*, 47, 461-470,
1460 <https://doi.org/10.1034/j.1600-0889.47.issue4.6.x>, 1995
1461

1462 Apel, K. and Hirt, H.: Reactive Oxygen Species: Metabolism, Oxidative Stress, and Signal
1463 Transduction, *Annual Review of Plant Biology* 2004, 55:1, 373-399,
1464 <https://doi.org/10.1146/annurev.arplant.55.031903.141701>, 2004
1465

1466 Austin, A. T., Méndez, M. S., and Ballaré, C. L.: Photodegradation alleviates the lignin
1467 bottleneck for carbon turnover in terrestrial ecosystems, *PNAS*, 13 (16), 4392-4397,
1468 <https://doi.org/10.1073/pnas.1516157113>, 2016
1469

1470 Baumgartner, M., Schilt, A., Eicher, O., Schmitt, J., Schwander, J., Spahni, R., Fischer, H.,
1471 and Stocker, T. F.: High-resolution inter-polar difference of atmospheric methane around the
1472 Last Glacial Maximum, *Biogeosciences*, 9, 3961–3977, [https://doi.org/10.5194/bg-9-3961-](https://doi.org/10.5194/bg-9-3961-2012)
1473 2012, 2012
1474

1475 Baumgartner, M., Kindler, P., Eicher, O., Floch, G., Schilt, A., Schwander, J., Spahni, R.,
1476 Capron, E., Chappellaz, J., Leuenberger, M., Fischer, H., and Stocker, T. F.: NGRIP
1477 CH₄ concentration from 120 to 10 kyr before present and its relation to a $\delta^{15}\text{N}$ temperature
1478 reconstruction from the same ice core, *Clim. Past*, 10, 903–920, [https://doi.org/10.5194/cp-](https://doi.org/10.5194/cp-10-903-2014)
1479 10-903-2014, 2014
1480

1481 Beck, J., Bock, M., Schmitt, J., Seth, B., Blunier, T., and Fischer, H.: Bipolar carbon and
1482 hydrogen isotope constraints on the Holocene methane budget, *Biogeosciences*, 15, 7155–
1483 7175, <https://doi.org/10.5194/bg-15-7155-2018>, 2018
1484

1485 Bernard, B., Brooks, J.M. and Sackett, W.M.: A geochemical model for characterization of
1486 hydrocarbon gas sources in marine sediments. In: 9th Annual Offshore Technology
1487 Conference, Houston, Texas, May 1977, 435–438 (OTC 2934), [https://doi.org/10.4043/2934-](https://doi.org/10.4043/2934-MS)
1488 MS, 1977
1489

1490 Biscaye, P. E., Grousset, F. E. , Revel, M., Van der Gaast, S., Zielinski, G. A., Vaars, A.
1491 and G. Kukla: Asian provenance of Glacial dust (stage 2) in the Greenland Ice Sheet Project 2
1492 Ice Core, Summit, Greenland, *J. Geophys. Res.*, 102, 26,765–26,781, 1997
1493

1494 Bock, M., Schmitt, J., Behrens, M., Möller, L., Schneider, R., Sapart, C. and Fischer, H.: A
1495 gas chromatography/pyrolysis/isotope ratio mass spectrometry system for high- precision dD
1496 measurements of atmospheric methane extracted from ice cores, *Rapid Commun. Mass*
1497 *Spectrom*, 24, 621–633, <https://doi.org/10.1002/rcm.4429>, 2010a
1498

1499 Bock, M., Schmitt, J., Blunier, T., Fischer, H., Möller, L. and Spahni, R.: Hydrogen
1500 Isotopes Preclude Marine Hydrate CH₄ Emissions at the Onset of Dansgaard- Oeschger
1501 Events, *Science*, 328, 1686-1689, <https://doi.org/10.1126/science.1187651>, 2010b
1502

1503 Bock, M., Schmitt, J., Beck, J., Schneider, R., and Fischer, H.: Improving accuracy and
1504 precision of ice core $\delta\text{D}(\text{CH}_4)$ analyses using methane pre-pyrolysis and hydrogen post-

1505 pyrolysis trapping and subsequent chromatographic separation, *Atmos. Meas. Tech.*, 7, 1999–
1506 2012, <https://doi.org/10.5194/amt-7-1999-2014>, 2014
1507
1508 Bock, M., Schmitt, J., Beck, J., Seth, B., Chappellaz, J. and Fischer, H.: Glacial/ interglacial
1509 wetland, biomass burning, and geologic methane emissions constrained by dual stable
1510 isotopic CH₄ ice core records, *PNAS*, 114 (29), E5778-E5786,
1511 <https://doi.org/10.1073/pnas.1613883114>, 2017
1512
1513 Bruhn, D., Mikkelsen, T. N., Øbro, J., Willats, W. G. T. and Ambus, P.: Effects of
1514 temperature, ultraviolet radiation and pectin methyl esterase on aerobic methane release from
1515 plant material, *Plant Biology*, 11, 43-48, <https://doi.org/10.1111/j.1438-8677.2009.00202.x>,
1516 2009
1517
1518 Campen, R. K., Sowers, T., and Alley, R. B.: Evidence of microbial consortia metabolizing
1519 within a low-latitude mountain glacier, *Geology*, 31, 231–234, [https://doi.org/10.1130/0091-7613\(2003\)031<0231:EOMCMW>2.0.CO;2](https://doi.org/10.1130/0091-7613(2003)031<0231:EOMCMW>2.0.CO;2), 2003
1520
1521
1522 Chappellaz, J., Blunier, T., Kints, S., Dällenbach, A., Barnola, J. M., Schwander, J., Raynaud,
1523 D. and Stauffer B.: Changes in the atmospheric CH₄ gradient between Greenland and
1524 Antarctica during the Holocene, *Geophys. Res. Lett.*, Volume 102, 15987-15997,
1525 <https://doi.org/10.1029/97JD01017>, 1997
1526
1527 Cheng, A. L. and Huang, W. L.: Selective adsorption of hydrocarbon gases on clays and
1528 organic matter, *Org. Geochem.*, 35, 413-423,
1529 <https://doi.org/10.1016/j.orggeochem.2004.01.007>, 2004
1530
1531 Dan, J., Kumai, T., Sugimoto, A. and Murase, J.: Biotic and abiotic methane releases from
1532 Lake Biwa sediment slurry, *Limnology* 5, 149–154, <https://doi.org/10.1007/s10201-004-0124-7>, 2004
1533
1534
1535 Derendorp, L., Holzinger, R., Wishkerman, A., Keppler, F., and Röckmann, T.: VOC
1536 emissions from dry leaf litter and their dependence on temperature, *Biogeosciences Discuss.*,
1537 7, 823–854, <https://doi.org/10.5194/bgd-7-823-2010>, 2010
1538
1539 Derendorp, L., Holzinger, R., Wishkerman, A., Keppler, F., and Röckmann, T.: Methyl
1540 chloride and C₂-C₅ hydrocarbon emissions from dry leaf litter and their dependence on
1541 temperature, *Atmospheric Environment*, 45, 3112-3119,
1542 <https://doi.org/10.1016/j.atmosenv.2011.03.016>, 2011
1543
1544 Dumelin, E.E. and Tappel, A.L.: Hydrocarbon gases produced during in vitro peroxidation of
1545 polyunsaturated fatty acids and decomposition of preformed hydroperoxides, *Lipids*, 12, 894,
1546 <https://doi.org/10.1007/BF02533308>, 1977
1547
1548 Dyonisius, M. N., Petrenko, V. V., Smith, A.M., Hua, Q., Yang, B., Schmitt, J., Beck, J.,
1549 Seth, B., Bock, M., Hmiel, B., Vimont, I., Menking, J. A., Shackleton, S. A., Baggenstos, D.,
1550 Bauska, T. K., Rhodes, R., Sperlich, P., Beaudette, R., Harth, C., Kalk, M., Brook, E. J.,
1551 Fischer, H., Severinghaus, J. P. and Weiss, R. F.: Old carbon reservoirs were not important in
1552 the deglacial methane budget, *Science*, 367(6480), 907-910,
1553 <https://doi.org/10.1126/science.aax0504>, 2020
1554

1555 Erhardt, T., Bigler, M., Federer, U., Gfeller, G., Leuenberger, D., Stowasser, O.,
1556 Röthlisberger, R., Schüpbach, S., Ruth, U., Twarloh, B., Wegner, A., Goto-Azuma, K.,
1557 Kuramoto, T., Kjær, H. A., Vallelonga, P. T., Siggaard-Andersen, M.-L., Hansson, M. E.,
1558 Benton, A. K., Fleet, L. G., Mulvaney, R., Thomas, E. R., Abram, N., Stocker, T. F., and
1559 Fischer, H.: High resolution aerosol concentration data from the Greenland NorthGRIP and
1560 NEEM deep ice cores, *Earth Syst. Sci. Data Discuss.*, 14, 1215–1231,
1561 <https://doi.org/10.5194/essd-14-1215>, 2022
1562

1563 Etiope, G. and Klusman, R. W.: Geologic emissions of methane to the atmosphere,
1564 *Chemosphere*, 49, 8, 777-789, [https://doi.org/10.1016/S0045-6535\(02\)00380-6](https://doi.org/10.1016/S0045-6535(02)00380-6), 2002
1565

1566 Etiope G., Martinelli G., Caracausi, A. and Italiano, F.: Methane seeps and mud volcanoes in
1567 Italy: gas origin, fractionation and emission to the atmosphere, *Geophys. Res. Lett.*, 34,
1568 <https://doi.org/10.1029/2007GL030341>, 2007
1569

1570 Etiope G., Lassey K. R., Klusman R. W. and Boschi, E.: Reappraisal of the fossil methane
1571 budget and related emission from geologic sources, *Geophys. Res. Lett.*, 35,
1572 <https://doi.org/10.1029/2008GL033623>, 2008
1573

1574 Frahry, G. and Schopfer, P.: Hydrogen peroxide production by roots and its stimulation by
1575 exogenous NADH, *Physiologia Plantarum*, 103, 395-404, <https://doi.org/10.1034/j.1399-3054.1998.1030313.x>, 1998
1576
1577

1578 Flückiger J., Blunier T., Stauffer B., Chappellaz M., Spahni R., Kawamura K., Schwander J.,
1579 Stocker T. F. and Dahl-Jensen D.: N₂O and CH₄ variations during the last glacial epoch:
1580 Insight into global processes, *Global Biogeochem. Cy* 18, 1020,
1581 <https://doi.org/10.1029/2003GB002122>, 2004
1582

1583 Fuhrer, K. and Legrand, M.: Continental biogenic species in the Greenland Ice Core Project
1584 ice core: Tracing back the biomass history of the North American continent, *J. Geophys. Res.*,
1585 102(C12), 26735– 26745, <https://doi.org/10.1029/97JC01299>, 1997
1586

1587 Georgiou, C. D., Sun, H. J., McKay, C. P., Grintzalis, K., Papapostolou, I., Zisimopoulos, D.,
1588 Panagiotidis, K., Zhang, G., Koutsopoulou, E., Christidis, G. E. and Margiolaki, I.: Evidence
1589 for photochemical production of reactive oxygen species in desert soils, *Nat.*
1590 *Commun.*, 6, 7100, <https://doi.org/10.1038/ncomms8100>, 2015
1591

1592 Giorio, C., Kehrwald, N., Barbante, C., Kalberer, M., King, A. C. F., Thomas, E. R., Wolff,
1593 E. W. and Zennaro, P.: Prospects for reconstructing paleoenvironmental conditions from
1594 organic compounds in polar snow and ice, *Quaternary Science Reviews*, 183, 1-22,
1595 <https://doi.org/10.1016/j.quascirev.2018.01.007>, 2018
1596

1597 Gu, Q., Chang, S. X., Wang, Z. P., Feng, J. C., Chen, Q. S. and Han, X. G.: Microbial versus
1598 non-microbial methane releases from fresh soils at different temperatures, *Geoderma*, 284,
1599 178-184, <https://doi.org/10.1016/j.geoderma.2016.08.027>, 2016
1600

1601 Han, C., Do Hur, S., Han, Y., Lee, K., Hong, S., Erhard, T., Fischer, H., Svensson, A. M.,
1602 Steffensen, J. P. and Vallelonga, P.: High-resolution isotopic evidence for a potential Saharan
1603 provenance of Greenland glacial dust. *Sci Rep* 8, 15582, <https://doi.org/10.1038/s41598-018-33859-0>, 2018
1604
1605

1606 Harris, E., Sinha, B., van Pinxteren, D., Tilgner, A., Wadinga Fomba, K., Schneider, J., Roth,
1607 A., Gnauk, T., Fahlbusch, B., Mertes, S., Lee, T., Collett, J., Foley, S., Borrmann, S., Hoppe,
1608 P. and Herrmann, H.: Enhanced Role of Transition Metal Ion Catalysis During In-Cloud
1609 Oxidation of SO₂, *Science*, 340, 727-730, <https://doi.org/doi:10.1126/science.1230911>, 2013
1610

1611 Helmig, D., Petrenko, V., Martinerie, P., Witrant, E., Röckmann, T., Zuiderweg, A.,
1612 Holzinger, R., Hueber, J., Thompson, C., White, J. W. C., Sturges, W., Baker, A., Blunier, T.,
1613 Etheridge, D., Rubino, M., and Tans, P.: Reconstruction of Northern Hemisphere 1950–2010
1614 atmospheric non-methane hydrocarbons, *Atmos. Chem. Phys.*, 14, 1463-1483,
1615 <https://doi.org/10.5194/acp-14-1463>, 2014
1616

1617 Hoheisel, A., Yeman, C., Dinger, F., Eckhardt, H., and Schmidt, M.: An improved method for
1618 mobile characterisation of $\delta^{13}\text{C}_{\text{CH}_4}$ source signatures and its application in Germany, *Atmos.*
1619 *Meas. Tech.*, 12, 1123–1139, <https://doi.org/10.5194/amt-12-1123-2019>, 2019.
1620

1621 Hurkuck, M., Althoff, F., Jungkunst, H. F., Jugold, A. and Keppler, F.: Release of methane
1622 from aerobic soil: An indication of a novel chemical natural process?, *Chemosphere*, 86, 684-
1623 689, <https://doi.org/10.1016/j.chemosphere.2011.11.024>, 2012
1624

1625 Ji L., Zhang T., Milliken K. L., Qu J. and Zhang X.: Experimental investigation of main
1626 controls to methane adsorption in clay-rich rocks, *Appl. Geochem.* 27, 2533–2545,
1627 <https://doi.org/10.1016/j.apgeochem.2012.08.027>, 2012
1628

1629 John, W. W. and Curtis, R. W.: Isolation and Identification of the Precursor of Ethane
1630 in *Phaseolus vulgaris* L., *Plant Physiology*, 59, 521–522, <https://doi.org/10.1104/pp.59.3.521>,
1631 1977
1632

1633 Jugold, A., Althoff, F., Hurkuck, M., Greule, M., Lenhart, K., Lelieveld, J., and Keppler, F.:
1634 Non-microbial methane formation in oxic soils, *Biogeosciences*, 9, 5291–5301,
1635 <https://doi.org/10.5194/bg-9-5291-2012>, 2012
1636

1637 Katagi, T.: Photoinduced Oxidation of the organophosphorus Fungicide Tolclofs-methyl on
1638 Clay Minerals, *J. Agric. Food Cham.*, 38, 1595-1600, 1990
1639

1640 Kaufmann, P. R., Federer, U., Hutterli, M. A., Bigler, M., Schüpbach, S., Ruth, U., Schmitt, J.
1641 and Stocker, T. F.: An Improved Continuous Flow Analysis System for High-Resolution
1642 Field Measurements on Ice Cores, *Environmental Science & Technology*, 42 (21), 8044-
1643 8050, <https://doi.org/10.1021/es8007722>, 2008
1644

1645 Keeling, C. D.: The concentration and isotopic abundance of carbon dioxide in rural areas,
1646 *Geochim. Cosmochim. Acta*, 13, 322–334 [https://doi.org/10.1016/0016-7037\(58\)90033-](https://doi.org/10.1016/0016-7037(58)90033-4)
1647 4.1958, 1958
1648

1649 Keeling, C. D.: The concentration and isotopic abundance of carbon dioxide in rural and
1650 marine air, *Geochim. Cosmochim. Acta*, 24, 277–298, [https://doi.org/10.1016/0016-](https://doi.org/10.1016/0016-7037(61)90023-0)
1651 7037(61)90023-0, 1961
1652

1653 Keppler, F., Hamilton, J. T. G., Braß, M. and Röckmann, T.: Methane emissions from
1654 terrestrial plants under aerobic conditions, *Nature* 439, 187–191,
1655 <https://doi.org/10.1038/nature04420>, 2006
1656

1657 Keppler, F., Hamilton, J. T. G., McRoberts, W. C., Vigano, I., Braß, M. and Röckmann, T.:
1658 Methoxyl groups of plant pectin as a precursor of atmospheric methane: evidence from
1659 deuterium labelling studies, *New Phytologist*, 178, 808-814, [https://doi.org/10.1111/j.1469-](https://doi.org/10.1111/j.1469-8137.2008.02411.x)
1660 [8137.2008.02411.x](https://doi.org/10.1111/j.1469-8137.2008.02411.x), 2008

1661 Kibanova, D., Trejo, M., Destailats, H. and Cervini-Silva, J.: Photocatalytic activity of
1662 kaolinite, *Catalysis Communications*, 12, 698-702,
1663 <https://doi.org/10.1016/j.catcom.2010.10.029>, 2011

1664 Köhler, P., Fischer, H., Schmitt, J., and Munhoven, G.: On the application and interpretation
1665 of Keeling plots in paleo climate research – deciphering $\delta^{13}\text{C}$ of atmospheric CO_2 measured in
1666 ice cores, *Biogeosciences*, 3, 539–556, <https://doi.org/10.5194/bg-3-539-2006>, 2006

1667 Lee, L. E., Edwards, J. S., Schmitt, J., Fischer, H., Bock, M. and Brook, E. J.: Excess methane
1668 in Greenland ice cores associated with high dust concentrations, *Geochim. Cosmochim. Acta*,
1669 270, 409-430, <https://doi.org/10.1016/j.gca.2019.11.020>, 2020

1670 Legrand, M., and Delmas, R.: Soluble Impurities in Four Antarctic Ice Cores Over the Last
1671 30000 Years, *Annals of Glaciology*, 10, 116-120,
1672 <https://doi.org/10.3189/S0260305500004274>, 1988

1673 Liu, J., Chen, H., Zhu, Q., Shen, Y., Wang, X., Wang, M., Peng, C.: A novel pathway of
1674 direct methane production and emission by eukaryotes including plants, animals and fungi:
1675 An overview, *Atmospheric Environment*, 115, 26,
1676 <https://doi.org/10.1016/j.atmosenv.2015.05.019>, 2015

1677 Liu, D., Yuan, P., Liu, H., Li, T., Tan, D., Yuan, W., He, H.: High-pressure adsorption of
1678 methane on montmorillonite, kaolinite and illite, *Applied Clay Science*, 85, 25-30,
1679 <https://doi.org/10.1016/j.clay.2013.09.009>, 2013

1680 Lupker, M., Aciego, S. M., Bourdon, B., Schwander, J., and Stocker, T. F.: Isotopic tracing
1681 (Sr, Nd, U and Hf) of continental and marine aerosols in an 18th century section of the Dye-3
1682 ice core (Greenland), *Earth Pla Sci Let*, 295, 277-286,
1683 <https://doi.org/10.1016/j.epsl.2010.04.010>, 2010

1684 McLeod, A. R., Newsham, K. K. and Fry, S.C.: Elevated UV-B radiation modifies the
1685 extractability of carbohydrates from leaf litter of *Quercus robur*, *Soil Biology and*
1686 *Biochemistry*, 39, Issue 1, 116-126, <https://doi.org/10.1016/j.soilbio.2006.06.019>, 2007

1687 McLeod, A.R., Fry, S.C., Loake, G.J., Messenger, D.J., Reay, D.S., Smith, K.A. and Yun, B.-
1688 W.: Ultraviolet radiation drives methane emissions from terrestrial plant pectins, *New*
1689 *Phytologist*, 180, 124-132, <https://doi.org/10.1111/j.1469-8137.2008.02571.x>, 2008

1690 Messenger, D.J., McLeod, A. R. and Fry, S.C.: The role of ultraviolet radiation,
1691 photosensitizers, reactive oxygen species and ester groups in mechanisms of methane
1692 formation from pectin, *Plant, Cell & Environment*, 32: 1-9, [https://doi.org/10.1111/j.1365-](https://doi.org/10.1111/j.1365-3040.2008.01892.x)
1693 [3040.2008.01892.x](https://doi.org/10.1111/j.1365-3040.2008.01892.x), 2009

1694 Milkov, A. V. and Etiope, G.: Revised genetic diagrams for natural gases based on a global
1695 dataset of >20,000 samples, *Organic Geochemistry*, 125, 109-120,
1696 <https://doi.org/10.1016/j.orggeochem.2018.09.002>, 2018

1708
1709 Mitchell, L., Brook, E., Lee, J. E., Buizert, C., and Sowers, T.: Constraints on the Late
1710 Holocene anthropogenic contribution to the atmospheric methane budget, *Science* 342, 964–
1711 966, <https://doi.org/10.1126/science.1238920>, 2013
1712
1713 Miteva V., Teacher C., Sowers T. and Brenchley, J.: Comparison of the microbial diversity at
1714 different depths of the GISP2 Greenland ice core in relationship to deposition climates,
1715 *Environ. Microbiol.*, 11, 640–656, <https://doi.org/10.1111/j.1462-2920.2008.01835.x>, 2009
1716
1717 Möller, L., Sowers, T., Bock, M., Spahni, R., Behrens, M., Schmitt, J., Miller, H. and Fischer,
1718 H.: Independent variations of CH₄ emissions and isotopic composition over the past 160,000
1719 years, *Nature Geosci*, 6, 885–890, <https://doi.org/10.1038/ngeo1922>, 2013
1720
1721 Mohnen, D.: Pectin structure and biosynthesis, *Current Opinion in Plant Biology*, 11, 266-
1722 277, <https://doi.org/10.1016/j.pbi.2008.03.006>, 2008
1723
1724 NEEM community members: Eemian interglacial reconstructed from a Greenland folded ice
1725 core, *Nature*, 493, 489–494, <https://doi.org/10.1038/nature11789>, 2013
1726
1727 Nicewonger, M. R., Verhulst, K. R., Aydin, M. and Saltzman, E. S.: Preindustrial
1728 atmospheric ethane levels inferred from polar ice cores: A constraint on the geologic sources
1729 of atmospheric ethane and methane, *Geophys. Res. Lett.*, 43,
1730 <https://doi.org/10.1002/2015GL066854>, 2016
1731
1732 Nicewonger, M. R., Aydin, M., Prather, M. J., and Saltzman, E.S.: Large changes in biomass
1733 burning over the last millennium inferred from paleoatmospheric ethane in polar ice cores,
1734 *Proc. Natl. Acad. Sci. USA*, 115 (49), 12413-12418,
1735 <https://doi.org/10.1073/pnas.1807172115>, 2018
1736
1737 North Greenland Ice Core Project members, High-resolution record of Northern Hemisphere
1738 climate extending into the last interglacial period, *Nature* 431, 147–151,
1739 <https://doi.org/10.1038/nature02805>, 2004
1740
1741 Pires, J., Bestilleiro, M., Pinto, M. and Gil, A.: Selective adsorption of carbon dioxide,
1742 methane and ethane by porous clays heterostructures, *Separation and Purification*
1743 *Technology*, 61, 161-167, <https://doi.org/10.1016/j.seppur.2007.10.007>, 2008
1744
1745 Price, P. B. and Sowers, T.: Temperature dependence of metabolic rates for microbial growth,
1746 maintenance, and survival, *P. Natl. Acad. Sci. USA* 101, 4631–4636,
1747 <https://doi.org/10.1073/pnas.0400522101>, 2004
1748
1749 Rohde, R. A., Price, P. B., Bay, R. C. and Bramall, N. E.: In situ microbial metabolism as a
1750 cause of gas anomalies in ice, *P. Natl. Acad. Sci. USA*, 105, 8667–8672,
1751 <https://doi.org/10.1073/pnas.0803763105>, 2008
1752
1753 Rhodes, R. H., Faïn, X., Stowasser, C., Blunier, T., Chappellaz, C., McConnell, J. R.,
1754 Romanini, D., Mitchell, L. E. and Brook, E. J.: Continuous methane measurements from a
1755 late Holocene Greenland ice core: Atmospheric and in situ signals, *Earth and Planetary*
1756 *Science Letters*, 368, 9-19, <https://doi.org/10.1016/j.epsl.2013.02.034>, 2013
1757

1758 Rhodes, R. H., Faïn, X., Brook, E. J., McConnell, J. R., Maselli, O. J., Sigl, M., Edwards, J.,
1759 Buizert, C., Blunier, T., Chappellaz, J., and Freitag, J.: Local artifacts in ice core methane
1760 records caused by layered bubble trapping and in situ production: a multi-site investigation,
1761 *Clim. Past*, 12, 1061–1077, <https://doi.org/10.5194/cp-12-1061-2016>, 2016
1762
1763 Ross, D. J. K. and Bustin, R. M.: The importance of shale composition and pore structure
1764 upon gas storage potential of shale gas reservoirs, *Mar. Petrol. Geol.*, 26, 916-927,
1765 <https://doi.org/10.1016/j.marpetgeo.2008.06.004>, 2009
1766
1767 Ruth, U., Wagenbach, D., Steffensen, J. P. and Bigler, M.: Continuous record of microparticle
1768 concentration and size distribution in the central Greenland NGRIP ice core during the last
1769 glacial period, *J. Geophys. Res.*, 108 (D3), 4098, <https://doi.org/10.1029/2002JD002376>,
1770 2003
1771
1772 Ruth, U., Bigler, M., Röthlisberger, R., Siggaard-Andersen, M.-L., Kipfstuhl, S., Goto-
1773 Azuma, K., Hansson, M. E., Johnsen, S. J., Lu, H., and Steffensen, J. P.: Ice core evidence
1774 for a very tight link between North Atlantic and east Asian glacial climate, *Geophys. Res.*
1775 *Lett.*, 34, L03706, doi:10.1029/2006GL027876, 2007
1776
1777 Schade, G. W., Hofmann, R.-M. and Crutzen, P. J.: CO emissions from degrading plant
1778 matter, *Tellus B: Chemical and Physical Meteorology*, 51:5, 889-908,
1779 <https://doi.org/10.3402/tellusb.v51i5.16501>, 1999
1780
1781 Schilt, A., Baumgartner, M., Blunier, T., Schwander, J., Spahni, R., Fischer, H., and Stocker,
1782 T. F.: Glacial–interglacial and millennial-scale variations in the atmospheric nitrous oxide
1783 concentration during the last 800,000 years, *Quat Sci Rev*, 29, 182-192,
1784 <https://doi.org/10.1016/j.quascirev.2009.03.011>, 2010
1785
1786 Schmitt, J., Seth, B., Bock, M. and Fischer, H.: Online technique for isotope and mixing ratios
1787 of CH₄, N₂O, Xe and mixing ratios of organic trace gases on a single ice core sample, *Atmos.*
1788 *Meas. Tech.*, 7, 2645–2665, <https://doi.org/10.5194/amt-7-2645-2014>, 2014
1789
1790 Smith, H. J., Wahlen, M., Mastroianni, D., and Taylor, K. C.: The CO₂ concentration of air
1791 trapped in GISP2 ice from the Last Glacial Maximum-Holocene transition, *Geophys Res Lett.*
1792 24, 1-4, <https://doi.org/10.1029/96GL03700>, 1997
1793
1794 Sugimoto, A., Dan, J., Kumai, T. and Murase J.: Adsorption as a methane storage process in
1795 natural lake sediment, *Geophys. Res. Lett.* 30, 2080, <https://doi.org/10.1029/2003GL018162>,
1796 2003
1797
1798 Svensson, A., Biscaye, P. E. and Grousset, F. E.: Characterization of late glacial continental
1799 dust in the Greenland Ice Core Project ice core, *J. Geophys. Res.-Atmos.*, 105, 4637–4656,
1800 <https://doi.org/10.1029/1999JD901093>, 2000
1801
1802 Tian, Y., Yan, C. and Jin, Z.: Characterization of Methane Excess and Absolute Adsorption in
1803 Various Clay Nanopores from Molecular Simulation, *Sci Rep* 7, 12040,
1804 <https://doi.org/10.1038/s41598-017-12123>, 2017
1805
1806 Tung, H. C., Bramall, N. E. and Price, P. B.: Microbial origin of excess methane in glacial ice
1807 and implications for life on Mars, *P. Natl. Acad. Sci. USA* 102, 18292–18296,
1808 <https://doi.org/10.1073/pnas.0507601102>, 2005

1809 Tung, H., Price, P., Bramall, N. and Vrdoljak G.: Microorganisms metabolizing on clay
1810 grains in 3-km-deep Greenland basal ice, *Astrobiology* 6, 69–86.
1811 <https://doi.org/10.1089/ast.2006.6.69>, 2006
1812
1813 Vigano, I., van Weelden, H., Holzinger, R., Keppler, F., McLeod, A., and Röckmann, T.:
1814 Effect of UV radiation and temperature on the emission of methane from plant biomass and
1815 structural components, *Biogeosciences*, 5, 937–947, <https://doi.org/10.5194/bg-5-937-2008>,
1816 2008
1817
1818 Vigano, I., Röckmann, T., Holzinger, R., van Dijk, A., Keppler, F., Greule, M., Brand, W. A.,
1819 Geilmann, H. and van Weelden, H.: The stable isotope signature of methane emitted from
1820 plant material under UV irradiation, *Atmospheric Environment*, 43, 5637-5646,
1821 <https://doi.org/10.1016/j.atmosenv.2009.07.046>, 2009
1822
1823 Vigano, I., Holzinger, R., Keppler, F., Greule, M., Brand, W. A., Geilmann, H., van Weelden,
1824 H. and Röckmann, T.: Water drives the deuterium content of the methane emitted from plants,
1825 *Geochimica et Cosmochimica Acta*, 74, 3865-3873, <https://doi.org/10.1016/j.gca.2010.03.030>,
1826 2010
1827 Wang, Z.P., Han, X.G., Wang, G.G., Song, Y. and Gulledge, J.: Aerobic methane emission
1828 from plants in the Inner Mongolia steppe, *Environmental Science & Technology* 42, 62– 68
1829 <https://doi.org/10.1021/es071224l>, 2008
1830
1831 Wang, Z.P., Xie, Z.Q., Zhang, B.C., Hou, L.Y., Zhou, Y.H., Li, L.H. and Han, X.G.: Aerobic
1832 and Anaerobic Nonmicrobial Methane Emissions from Plant Material, *Environmental Science*
1833 *& Technology* 2011 45 (22), 9531-9537, <https://doi.org/10.1021/es2020132>, 2011
1834
1835 Wang, B., Hou, L., Liu, W. and Wang, Z.: Non-microbial methane emissions from soils,
1836 *Atmospheric Environment*, 80, 290–298, <https://doi.org/10.1016/j.atmosenv.2013.08.010>,
1837 2013
1838
1839 Wang, B., Lerdau, M. and He, Y.: Widespread production of nonmicrobial greenhouse gases
1840 in soils, *Glob Change Biol.*, 23:4472–4482, <https://doi.org/10.1111/gcb.13753>, 2017
1841
1842 Watanabe, M., Watanabe, Y., Kim, Y. S., Koike, T.: Dark aerobic methane emission
1843 associated to leaf factors of two *Acacia* and five *Eucalyptus* species, *Atmospheric*
1844 *Environment*, 54, 277-281, <https://doi.org/10.1016/j.atmosenv.2012.02.012>, 2012
1845
1846 Wehr, R. and Saleska, S. R.: The long-solved problem of the best-fit straight line: application
1847 to isotopic mixing lines, *Biogeosciences*, 14, 17–29, <https://doi.org/10.5194/bg-14-17-2017>,
1848 2017.
1849
1850 Whiticar, M. J.: Carbon and hydrogen isotope systematics of bacterial formation and
1851 oxidation of methane, *Chemical Geology*, 161, 291-314, [https://doi.org/10.1016/S0009-](https://doi.org/10.1016/S0009-2541(99)00092-3)
1852 [2541\(99\)00092-3](https://doi.org/10.1016/S0009-2541(99)00092-3), 1999
1853
1854 Wu, F., Li, J., Peng, Z., Deng, N.: Photochemical formation of hydroxyl radicals catalyzed by
1855 montmorillonite, *Chemosphere*, 72, 407-413,
1856 <https://doi.org/10.1016/j.chemosphere.2008.02.034>, 2008
1857
1858 York, D.: Least squares fitting of a straight line with correlated errors, *Earth and Planetary*
1859 *Science Letters*, 5, 320-324, [https://doi.org/10.1016/S0012-821X\(68\)80059-7](https://doi.org/10.1016/S0012-821X(68)80059-7), 1968

1860
1861 York, D., Evensen, N. M., Martinez, M. L., and De Basabe Delgado, J.: Unified equations for
1862 the slope, intercept, and standard errors of the best straight line, *Am. J. Phys.* 72, 367–375,
1863 <https://doi.org/10.1119/1.1632486>, 2004